

LEVELS IN ⁹⁵Tc

LEVELS IN ^{95}Tc

by

KATHARINE ALLAN MARSHALL, B.Sc.



A Thesis

Submitted to the Faculty of Graduate Studies
in Partial Fulfillment of the Requirements

for the Degree of
Master of Science

McMaster University

September 1976

©

K[^]

ALLAN

MASTER OF SCIENCE (1976)
(Physics)

McMASTER UNIVERSITY
Hamilton, Ontario

TITLE: Levels in ^{95}Tc

AUTHOR: Katharine Allan Marshall, B.Sc. (McMaster University)

SUPERVISOR: Dr. M. W. Johns

NUMBER OF PAGES: ix, 60

ABSTRACT

The structure of the nucleus ^{95}Tc was studied using the $(\alpha, 2n)$ reaction on ^{93}Nb . Excitation functions and gamma-gamma coincidence experiments were used to establish the decay scheme. The angular distributions of the gamma rays involved in the decays were also measured. From these data, energies, spins, and parities for states in ^{95}Tc have been established. A positive parity band and a negative parity band have been specifically emphasised, and interpreted in terms of the rotation aligned model.

ACKNOWLEDGEMENTS

I wish to thank my supervisor and research director, Dr. M. W. Johns, and also both past and present members of his research group; their assistance was certainly appreciated.

May I also extend my gratitude to the members of the Tandem Accelerator Laboratory: faculty, students, and staff with whom I have had many useful discussions during my course of study.

I would like to express my thanks to my sister Mary, for her dexterous typing of this thesis.

My special thanks go to Dr. J. V. Thompson, for his astute suggestions and observations, and his unfailing interest.

Finally, I would like to dedicate this work to my Mother and Father.

TABLE OF CONTENTS

		Page
CHAPTER 1	INTRODUCTION	1
1.1	Shell Model	1
1.2	Collective Motion	4
1.3	Applications to ^{95}Tc	6
CHAPTER 2	EXPERIMENTAL TECHNIQUES	8
2.1	Target Preparation	8
2.2	Excitation Function	8
2.3	Energy Measurements	11
2.4	Angular Distribution Measurements	12
2.5	Gamma-Gamma Coincidence Measurements	14
CHAPTER 3	EXPERIMENTAL RESULTS AND DISCUSSION	21
3.1	Gamma Ray Singles Measurements	22
3.2	Gamma-Gamma Coincidence Results	29
3.3	Presentation and Discussion of the Level Scheme	34
3.3.1	The Positive Parity Band	36
3.3.2	The Negative Parity Band	40
3.3.3	The 957.3, 1549.8, 2184.3, and 2907.5 keV Levels	53
3.3.4	The Shell Model Levels	55
3.3.5	The 1280, 2120, 2231.1, and 2475.1 keV Levels	56

TABLE OF CONTENTS (continued)

	Page
3.4 Comparison with Other Workers	56
3.5 Subsequent Investigations	57
REFERENCES	59

LIST OF TABLES

Number		Page
2.1	Possible Reactions and Q-Values	10
2.2	Explanation of the Code Used in Figure 2.3	17
3.1	Transitions in ^{95}Tc	24
3.2	Corrections for Detector Solid Angle	30
3.3	Coincidence Probabilities	31
3.4	Gamma Rays Appearing in Coincidence with the 510.8 keV Gamma Ray Transition	45

LIST OF FIGURES

Number		Page
2.1	A diagram of the detector geometry for the gamma-gamma coincidence experiment	15
2.2	A photograph showing the experimental set-up with the detectors in place	15
2.3	A block diagram of the coincidence circuit	16
2.4	An example of the output of PKCAL	19
3.1	The gamma ray spectrum of ^{95}Tc	23
3.2	The level scheme of ^{95}Tc	35
3.3	The spectrum in coincidence with a gate set on the 1031.8 keV transition	37
3.4	The angular distributions of the six transitions in the positive parity band	38
3.5	The excitation functions of the six transitions in the positive parity band	39
3.6	A comparison of the positive parity band of ^{95}Tc with levels in the core nucleus ^{94}Mo	41
3.7	The spectrum in coincidence with a gate set on the 811.2 keV photopeak	43
3.8	The spectrum in coincidence with the sum of gates set on the 487.8 and 745.1 keV photopeaks	44
3.9	The angular distributions of six transitions in the negative parity band	47

LIST OF FIGURES (continued)

Number		Page
3.10	The angular distributions of eight transitions which effect connections with the two major bands	48
3.11	The excitation functions of six transitions in the negative parity band	50
3.12	A comparison of the negative parity band of ^{95}Tc with levels in the nucleus ^{96}Mo	51
3.13	A plot of energy as a function of $J(J + 1)$ showing the negative parity band of ^{95}Tc and two bands of ^{96}Mo	52
3.14	The spectrum in coincidence with a gate set on the 957.3 keV photopeak	54

CHAPTER 1

INTRODUCTION

There have been several theoretical and experimental studies undertaken in recent years to gain an understanding of the properties of systems with multiparticle configurations. The region around mass 90 provides a useful example of such investigations. The odd technetium isotopes are particularly interesting, since the last few protons primarily occupy the $(g_{9/2})^3$ configuration.

This section describes some of the nuclear models pertinent to this mass region, and in this context, some of the general features of these nuclei, particularly ^{95}Tc .

1.1 Shell Model

The basic assumption of the shell model is that each nucleon behaves as an independent particle in an orbit determined by a central potential, created from the averaged interactions of all other nucleons. The orbital angular momentum ℓ of each nucleon is a constant of the motion for the central potential, and each value of ℓ gives rise to a series of energy levels.

It is found experimentally, that large gaps occur in the level spacings with corresponding discontinuities in nuclear properties, such

as binding energy, neutron capture cross-section, and angular momentum. The shell model interprets these gaps in terms of shell closures, which occur when the number of protons or neutrons corresponds to one of the "magic numbers": 2, 8, 20, 50, 82, and 126. This experimentally observed phenomenon can be interpreted in terms of a spin-orbit coupling force, of the form $V(r)\underline{l}\cdot\underline{s}$ where $V(r)$ describes the radial dependence, and $\underline{l}\cdot\underline{s}$ are the orbital and intrinsic angular momenta. By adjusting the strength of the $\underline{l}\cdot\underline{s}$ coupling, the energy gaps which occur at the magic numbers can be produced. The spin-orbit force has the effect of splitting a single $n\ell$ state into two states, namely $j = \ell \pm \frac{1}{2}$. The level with the larger j is more tightly bound. Since the magnitude of the splitting increases with the value of ℓ , the interaction causes levels with different values of (n, ℓ, j) to overlap, thus creating closed shells.

The extreme single-particle model, which is the simplest form of the shell model assumes that the proton and neutron states fill independently. The nucleons in the ground state have dynamically paired motions (each pair couples to zero angular momentum), with the result that the last unpaired nucleon if present, dominates the nuclear properties. All states which can be formed from k particles with the same quantum numbers (n, ℓ, j) are degenerate.

A more realistic model considers the internucleon forces among particles in unfilled orbitals, and treats the nucleons in closed shells as an inert core. The so-called residual interaction in this extended single-particle model is strong enough to remove the above

degeneracies, but not so strong in comparison with the spin-orbit force that j ceases to be a good quantum number for each nucleon. It is difficult however, to determine the exact form of the residual interaction, because not even the two nucleon interaction is well understood. It is very strong at small distances though, and so can be expected to modify the nuclear wavefunction where two nucleons are very close together. Therefore, to use this model, a modified Hamiltonian which contains effective two-body interactions between nucleons must be considered. The effective interactions can be replaced by a simple phenomenological interaction, obtained using experimental data from a group of nuclei for which the same configurations occur. The calculated matrix elements can then be used to predict properties of other nuclei. As an example, the Hamiltonian for a system of nucleons outside a core nucleus (e.g. ${}_{40}^{90}\text{Zr}_{50}$) can be written (Bhatt and Ball 1964) as

$$H = H_{\text{core}} + \left(\sum_p H_{p\text{-core}} + \sum_n H_{n\text{-core}} \right) + \left(\sum_{\text{pairs}} H_{pp} + \sum_{\text{pairs}} H_{nn} \right) + \sum_{\text{pairs}} H_{pn}$$

The first term represents the total interaction between nucleons inside the core; the second part represents the interaction of the extra-core protons and neutrons with the core. The third and fourth terms represent the residual interactions between the extra-core proton, neutron, and proton neutron pairs. The nn , pp , and pn effective interactions are determined from experimental data.

An important phenomenon which affects the filling of shell model levels is that of pairing. Two nucleons with the same (n, l, j)

quantum numbers and opposite intrinsic spin interact strongly to form a "zero coupled pair." This rather stable pair causes an increase in nuclear binding energy, over and above the "individual" binding energies. The gain in energy increases with the angular momentum j .

Experimentally, it is found that when two shell model states of different angular momentum are close together in energy, the state of higher angular momentum will tend to fill in pairs preferentially. As an example, the shell model predicts that the $1g_{9/2}$ orbital has a slightly higher excitation than the $2p_{1/2}$ orbital. However, due to the pairing effect, the $1g_{9/2}$ orbital will be filled with pairs of particles before the $2p_{1/2}$ orbital is completely filled. This effect is particularly important in the technetium isotopes.

1.2 Collective Motion

Nuclei with partially filled shells have been shown to possess large quadrupole moments, level structures indicative of a rigid rotor, and electric quadrupole transition rates much faster than a simple shell model can explain. These data necessitate a model which includes collective nuclear motion: that is, a model which considers that a large number of particles may be involved in cooperative modes of motion of an aspherical nature.

The collective theory developed by Bohr and Mottelson (1953), treated the nucleus as an incompressible, deformable liquid drop interacting with the extra nucleons of the unfilled shell.

Oscillations about a spherical shape can be written in terms of spherical harmonics

$$R(\theta, \phi) = R_0 \left[1 + \sum_{\lambda=0}^{\infty} \sum_{\mu=-\lambda}^{\lambda} \alpha_{\lambda\mu} Y_{\lambda}^{\mu}(\theta, \phi) \right]$$

where R_0 is the radius of the undistorted nuclear surface, and the $\alpha_{\lambda\mu}$ are the deformation parameters. Collective motions are expressed by allowing $\alpha_{\lambda\mu}$ to vary in time. Expressions for the kinetic and potential energies can be obtained, hence relationships for the frequency of vibration of the surface ω_{λ} . These vibrations are phonons, of order λ , and have an angular momentum λ , parity $(-1)^{\lambda}$, and an energy $\hbar\omega_{\lambda}$ associated with them. This model predicts the level structures of even-even nuclei with a few extra-core nucleons very well.

A more physical notation expresses the vibrational behaviour in terms of two other parameters, β (a measure of the total nuclear deformation) and γ (a measure of the asymmetry), which are related to the $\alpha_{\lambda\mu}$'s.

When the nucleus has a large permanent deformation caused by a large number of particles outside a closed shell, the nucleus may experience both rotations and vibrations. The characteristic rotational level structure can be derived by considering the nucleus to be a rigid rotor. Here, rotational and vibrational motions are treated separately in the Hamiltonian. The energy associated with the rotational motion of a state involving an intrinsic energy ϵ_K is given by

$$E = \epsilon_K + \frac{\hbar^2}{2\mathcal{I}} [J(J+1) - K^2] - BJ^2(J+1)^2$$

The last term results from a weak-coupling between rotational and vibrational modes of motion. Rotational bands can be built up on vibrational states as well as on particle states.

Odd nuclei have non-zero intrinsic spins, which necessitate the consideration of coupling of the particle motions with the collective motions. Therefore, terms involving the component of the particle's angular momentum (j) along the symmetry axis (Ω) and involving rotational particle coupling must be added to the above expression. The latter term is negligible except in two special cases. If two close-lying states differ by one unit in K , important perturbations can result. The other case where the RPC term is important is in a rotational band for which $\Omega = \frac{1}{2}$.

1.3 Applications to ^{95}Tc

The technetium isotopes have 43 protons. If $^{88}_{38}\text{Sr}_{50}$ is considered as the core nucleus, the $1f_{5/2}$ and $2p_{3/2}$ subshells will be completely filled, and the five extra-core protons will be distributed among the $2p_{1/2}$ and $1g_{9/2}$ subshells. The extreme single-particle model predicts that the forty-third proton will be found in the $1g_{9/2}$ subshell. Considerable energy can be gained if the protons in the $1g_{9/2}$ subshell are paired, leaving the unpaired proton in the $2p_{1/2}$ subshell. This causes the $g_{9/2}$ and $p_{1/2}$ states to be found close together in the level scheme. In fact the $(1g_{9/2})^3(2p_{1/2})^2$ configuration gives rise to the $9/2^+$ ground state, and the $(1g_{9/2})^4(2p_{1/2})^1$ configuration to an isomeric state (half-life 61 days) at 38.9 keV with spin

$1/2^-$ (Tucker and Hein 1970).

The shell model predicts spins up to $21/2^+$ only, from the $(g_{9/2})^3$ configuration. Hence any higher spins if present, would indicate collective motion. The Tc isotopes from mass 93 to 101, should actually be expected to span a transitional region, having an increasingly collective nature as neutrons are added. The high-spin states which may exemplify this feature in ^{95}Tc , can be populated using the $(\alpha, 2n)$ reaction on ^{93}Nb .

The coupling of a three-quasiparticle or three-quasihole cluster to quadrupole vibrations of the core has recently been investigated (Paar 1973). The conclusion was that there exist both quasivibrational and quasirotational features in the spectrum of ^{107}Ag . The $(g_{9/2})^3$ configuration in ^{95}Tc is very analogous to the $(g_{9/2})^{-3}$ situation in ^{107}Ag .

An alternate model which may explain the high-spin states equally as well as the cluster-core coupling model is the rotational aligned model (Stéphens et al. 1972, 1973). This model predicts a band of rotation aligned states with spins differing by 2 units of angular momentum, having the same relative spacings as those of the corresponding bands in neighbouring even deformed nuclei.

It is therefore highly interesting to consider the relative merits of these two models when applied to the high spin structure of ^{95}Tc .

CHAPTER 2

EXPERIMENTAL TECHNIQUES

A major task of the experimenter is to perform careful experiments, and having done this, he must then devise systematic and accurate methods to handle his experimental data. This section describes the experiments, and the methods used to analyse the acquired data.

2.1 Target Preparation

Niobium is a mono-isotopic nucleus with atomic weight 92.91 u. It occurs as a ductile metal, and so is particularly amenable to rolling, for fabrication of self-supporting targets.

A piece of Nb foil, approximately 5 mm x 5 mm x .001 inch (i.e. 21.8 mg cm⁻²), was first cleaned in acetone and then washed several times in HNO₃. The foil was then rolled to a thickness of about 5 mg cm⁻². Targets were rolled from this to suitable thicknesses, in the range 1 to 5 mg cm⁻².

2.2 Excitation Function

The yield of an (α ,xn) reaction is a well defined function of the bombarding energy for each value of x. As the excitation energy

is increased, these functions rise sharply from zero to a maximum, and decrease slowly. The threshold and peak yields depend strongly on the Q-value of the reaction. Therefore, a measurement of the excitation function of a particular gamma ray will give a good indication to which nucleus that gamma ray belongs. It may also indicate whether the radiation is coming from a state of high or low spin.

The $(\alpha, 2n)$ reaction on ^{93}Nb is endoergic with a Q-value of -14.9 MeV. Several other reactions will also proceed over the range of incident energies required for the excitation function. The possible reactions are tabulated along with their Q-values in Table 2.1. Not all of these reactions will be seen since the cross-section for reactions such as $(\alpha, ^3\text{He})$ is very small. Nevertheless, it was felt that nuclei such as ^{94}Mo could be populated by the (α, dn) or $(\alpha, p2n)$ reaction.

The Nb target, of thickness 1.3 mg cm^{-2} was mounted on a Pb holder and placed in the thin walled target chamber. Target backing was not required since the beam was stopped further down the line in a well-shielded beam dump. A planar 14 cc Ge(Li) detector was placed 55° from the beam, and approximately 4 cm from the target. Gamma ray spectra were collected using a PDP-9 computer at incident energies of 27.0, 24.5, 22.0, 19.5, and 17.0 MeV. The current in each case was approximately 1.5 nanoamps. The integrated beam current was recorded for each run, to be used to normalize the spectra.

TABLE 2.1

Possible Reactions and Q-values

${}^{93}\text{Nb}(\alpha, 2n){}^{95}\text{Tc}$	-14.9 MeV
${}^{93}\text{Nb}(\alpha, n){}^{96}\text{Tc}$	- 7.0 MeV
${}^{93}\text{Nb}(\alpha, 3n){}^{94}\text{Tc}$	-24.8 MeV
${}^{93}\text{Nb}(\alpha, p){}^{96}\text{Mo}$	- 3.3 MeV
${}^{93}\text{Nb}(\alpha, d){}^{95}\text{Mo}$	-10.2 MeV
${}^{93}\text{Nb}(\alpha, t){}^{94}\text{Mo}$	-11.3 MeV
${}^{93}\text{Nb}(\alpha, {}^3\text{He}){}^{94}\text{Nb}$	-13.3 MeV
${}^{93}\text{Nb}(\alpha, \alpha){}^{93}\text{Nb}$	0

Intensities of each gamma ray were extracted for each excitation energy using the programme JAGSPOT. This programme was originally written at the Chalk River Nuclear Laboratories (Williams and MacPherson 1968, Graham et al. 1972). The current version used at McMaster has been well described (Cook 1972); the only subsequent modification being that up to 10 peaks can now be fitted, in a window width of 200 channels maximum.

The peak areas were normalized using the integrated beam current, and were plotted against the excitation energy to give excitation functions.

Excitation functions relative to the 336 keV gamma ray were also plotted. This radiation is known from decay work (Xenoulis and Sarantites 1973, Krämer and Huber 1973), to be a transition from a $7/2^+$ level to the $9/2^+$ ground state of ^{95}Tc . The slope of such relative excitation functions provided some indication of the level of excitation of the initial state for the gamma ray under investigation, since levels with high spin require more excitation energy for population to occur.

2.3 Energy Measurements

It is essential to obtain accurate energies of the gamma ray transitions so that a level scheme can be established. This is usually done by using standard radioactive sources for which the energies are well known. The peak positions being studied are then compared with those of the known peaks.

Reaction and radioactive source spectra were collected with the detector [planar 14 cc Ge(Li)] at 55 degrees to the beam. The detailed form of the calibration curve was determined from a spectrum containing only radioactive sources of ^{57}Co , ^{60}Co , ^{137}Cs , ^{241}Am , and ^{152}Eu . The stronger transitions in the reaction were then measured against the lines in ^{57}Co and ^{60}Co by simultaneously recording a spectrum from these radioactive sources and the $(\alpha, 2n)$ reaction. Finally, the in-beam spectrum was recorded alone, with the stronger lines now available as internal standards.

2.4 Angular Distribution Measurements

An (α, xn) reaction will produce strong alignment in the residual nucleus. This is because all of the angular momentum (about 16 units of \hbar) brought into the reaction is in the $m = 0$ substate. Thus, radiation emitted from the residual nucleus, changing its state from initial spin J_i to final spin J_f , may show a strong anisotropy in the angular distribution, which can be expressed in terms of even Legendre Polynomials as

$$W(\theta) = A_0 + A_2 P_2(\cos\theta) + A_4 P_4(\cos\theta)$$

where θ is the angle of emission with respect to the quantisation axis (beam direction). The A_2 and A_4 coefficients can be found by fitting the experimental data to this expansion. When assumptions concerning initial and final spins and populations are made, theoretical angular distribution functions can also be calculated. These can then be compared with the experimental data, and the goodness of fit

used to determine acceptable combinations of J_i and J_f .

The target used was a Nb foil, 1.3 mg cm^{-2} thick, mounted on a tantalum holder. In order to obtain a 0 degree measurement, it was necessary to stop the beam at the target position. This was accomplished using a piece of bismuth approximately 300 mg cm^{-2} thick, mounted on the back of the target. The target was oriented in the target chamber; its normal made an angle of 48° to the beam direction. An incident energy of 26 MeV, with a current of 2.5 nanoamps was used. A 14 cc planar Ge(Li) detector was used as the moving counter. It was placed 14.0 cm from the target, and situated so that it could see through the back of the target. A 1 cc true coaxial Ge(Li) detector placed at 90° to the beam direction was used as a monitor counter for normalization purposes. The integrated beam current and time for each angle were also recorded as a check on the monitor.

The yields at the seven angles, 0, 90, 55, 15, 75, 30, and 45 degrees were measured, for approximately 3 hours per angle. This order was used to avoid any systematic build-up of activity which could mistakenly be interpreted as an angular distribution. The advantage of having the data for the 0 degree angle far outweighed the presence of the impurity lines in the spectrum, which were created by the Bi backing. The angular distribution data were collected and handled in the same way as the excitation function data. The spectra were normalized using the 363.3 keV transition from ^{95}Tc in the monitor spectra.

2.5 Gamma-Gamma Coincidence Measurements

The coincidence method is a powerful tool for establishing a unique level scheme, since it shows which gamma transitions are genetically related. Gamma rays are observed in two detectors placed in a fixed position relative both to the target and to each other. The coincidence circuit picks out pairs of events which arrive within the resolving time of the circuit (typically 50 nanoseconds). This technique selects as true coincidences, those events which form cascading transitions in a nucleus. By setting a gate on a single peak in the output of one detector, the spectrum from the second detector of all events in coincidence with the gate is obtained.

Two true coaxial Ge(Li) detectors, with volumes 37 cc and 50 cc, were positioned in a geometry 90 degrees to the beam axis and approximately 120 degrees to each other. The distance from the target to the detectors was 3.6 cm and 3.0 cm respectively. An incident beam with energy 26 MeV was used to bombard the 4.5 mg cm^{-2} Nb target. No backing was required since the beam was stopped in a well-shielded beam dump further down the beam line. The chamber used was the same as that for the excitation function. A shield of Pb, 1.6 cm thick, was placed between the detectors to minimise inter-crystal scattering. This geometry is shown in Figure 2.1 and Figure 2.2. The electronics used are shown in a schematic, Figure 2.3.

Fifteen 2400 foot magnetic tapes of coincidence data were collected, each containing 1.4 million coincidence events, using an address-recording programme which handled the three parameters: energy, energy,

FIGURE 2.1

A diagram of the detector geometry for the gamma-gamma coincidence experiment (beam direction is out of the page).

FIGURE 2.2

A photograph showing the experimental set-up with the detectors in place.

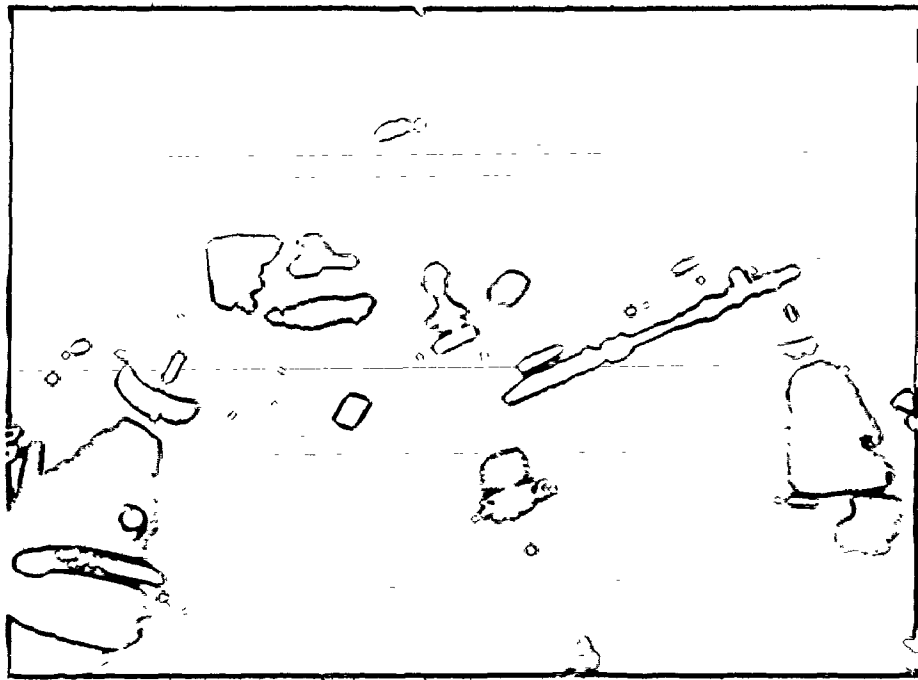
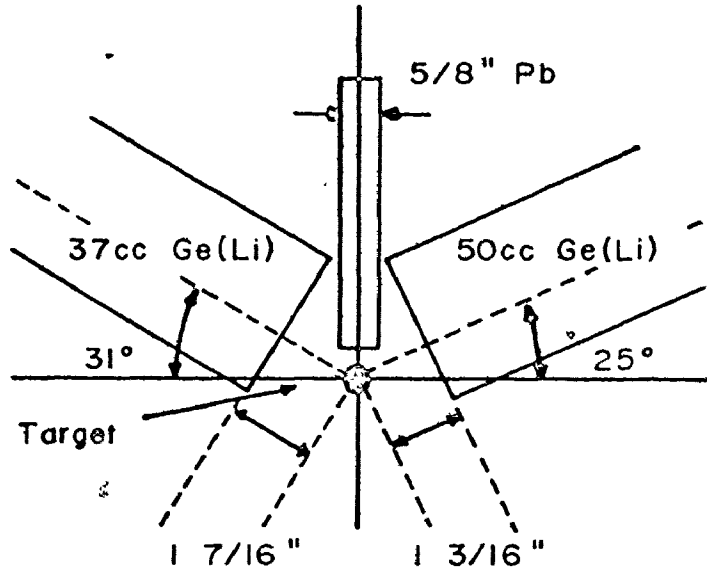


FIGURE 2.3

A block diagram of the coincidence circuit.

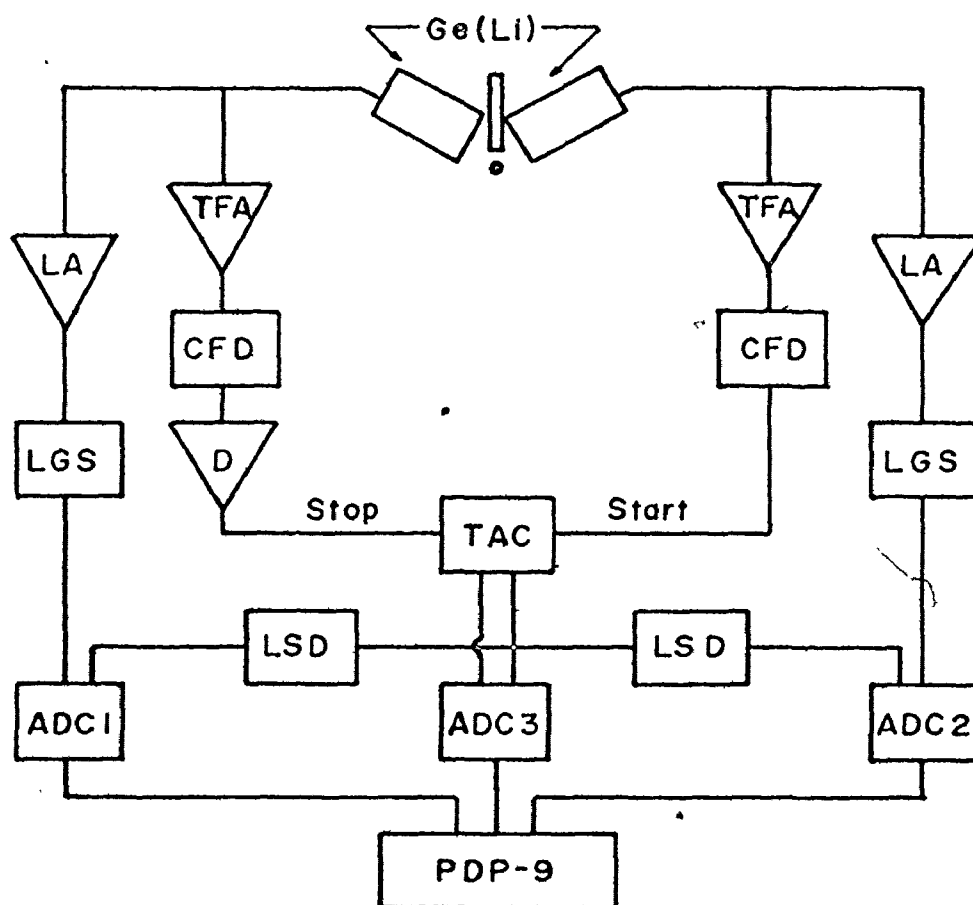


TABLE 2.2

Explanation of the Code Used in Figure 2.3

Abbreviation	Explanation
LA	linear amplifier (ORTEC 452, TC 203 BLR)
LGS	linear gate and stretcher (ORTEC 442)
TFA	timing filter amplifier (ORTEC 454)
CFD	constant fraction discriminator (ORTEC 453)
D	delay (ORTEC 425)
TAC	time to pulse height converter (ORTEC 467)
LSD	logic shaper and delay (CI 1455)
PDP-9	digital equipment corporation, computer

and time. Efficiency curves for each detector gated by the timing circuit were obtained, using a ^{182}Ta radioactive source, which emits a large number of lines of known intensity.

Since the 37 cc detector had better resolution, this spectrum was projected, so that gates could be set on each peak to be sorted. In the cases where there were several close-lying peaks in the spectrum, the programme JAGSPOT was used to fit each peak. The parameters calculated by JAGSPOT were then used in another programme (PKCAL), to define the profiles of each component in the multiplet. Gates could then be set on any one component, minimising the contributions from close-lying neighbours. An example of the output from PKCAL, and the windows subsequently set is shown in Figure 2.4. Having set windows on each peak and suitable upper and lower backgrounds for each, the data were then sorted on the PDP-15 computer.

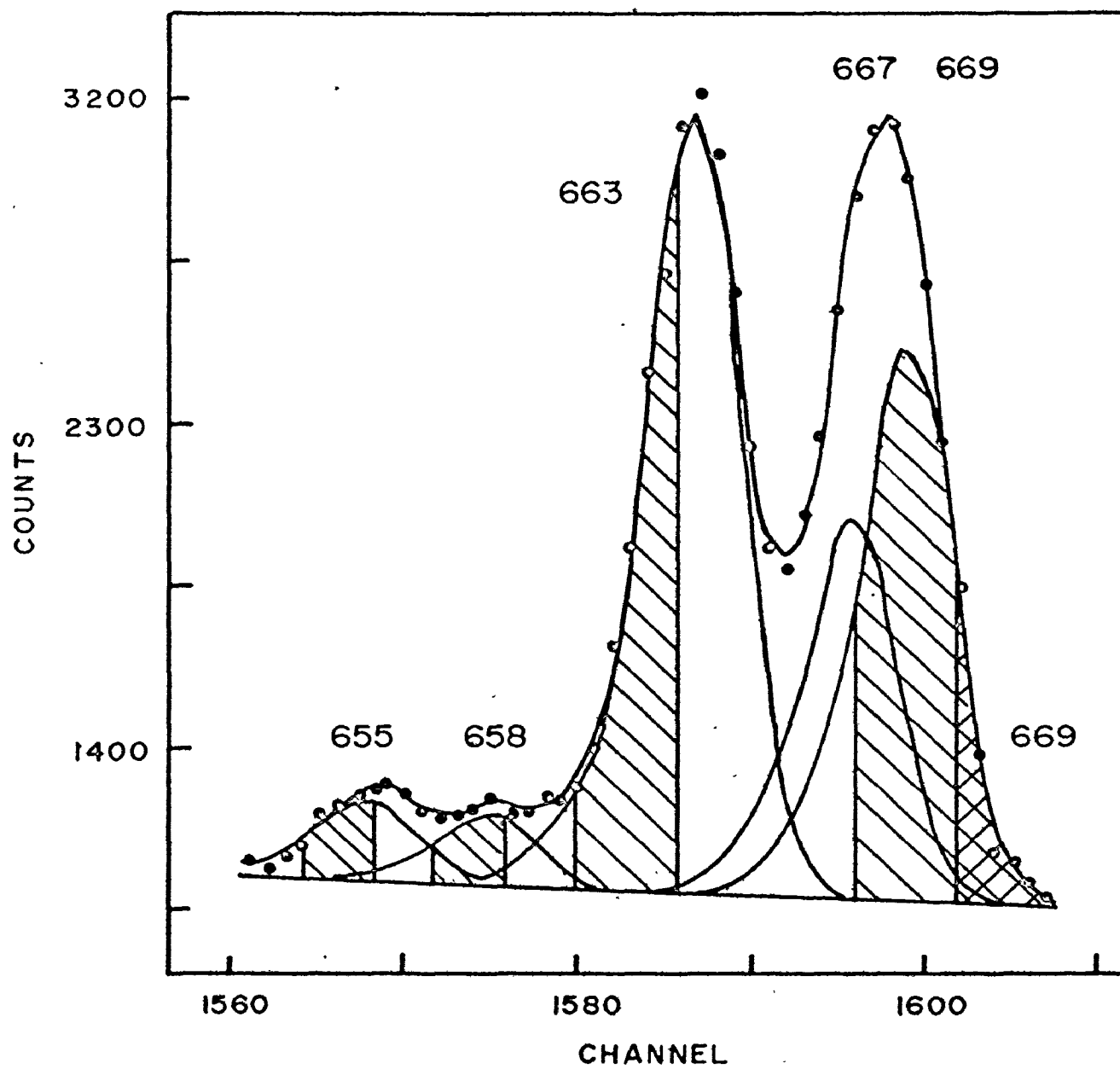
The areas of the peaks in each of the ninety-six gated spectra were calculated using the programme SOFT. These areas were used to obtain coincidence probabilities between gamma rays observed in the gated spectrum and the gating transition. The number of coincidence events between the full energy peaks of γ_i and γ_j is given by

$$N_{ij} = N_0 (\epsilon\omega)_i (\epsilon\omega)_j C_{ij}$$

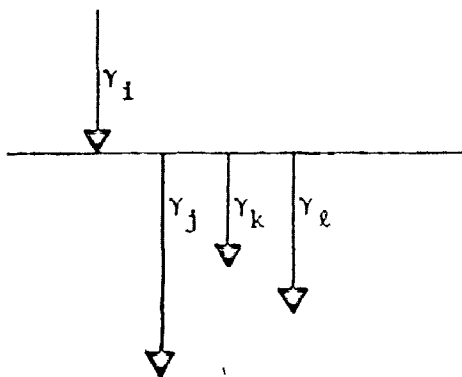
where $(\epsilon\omega)_i$ and $(\epsilon\omega)_j$ are the corresponding efficiencies and C_{ij} is the coincidence probability. N_0 is proportional to the total charge collected during the experiment, and is related through the cross-section and target thickness to the total number of gamma rays emitted from the

FIGURE 2.4

An example of the output of PKCAL, showing the envelope fitting the experimental data and the individual peaks in the multiplet. The coincidence gates subsequently set are shown by the hatch marks.



target during the experiment. N_0 was determined from several strong cascades, for which the coincidence probabilities were regarded as known.



For a situation such as that shown in the diagram at the left, the experimental coincidence probability between γ_1 and γ_j is given by

$$C_{ij} = C_{ji} = I_i b_j$$

where I_i is the intensity of the populating transition and b_j is the fraction of that intensity de-exciting the level through γ_j . This fraction is equal to the intensity of γ_j divided by the total intensity (including internal conversion) proceeding from the level.

Having established a level scheme from the coincidence data, the experimental coincidence probabilities were compared with those expected from the decay scheme to test its validity.

CHAPTER 3

EXPERIMENTAL RESULTS AND DISCUSSION

This work is a continuation of the study of the structure of the odd mass technetium isotopes (Cook 1972). Since the investigation of ^{95}Tc was undertaken, three works studying the nucleus using the $(\alpha, 2n)$ reaction have been published (Shibata et al. 1974, Hippe et al. 1975, and Sarantites 1975).

Shibata studied low-lying states in ^{95}Tc with particular emphasis on the core multiplet states which can be formed by the coupling of a $1g_{9/2}$ proton to the quadrupole phonon state of the core. Hippe added higher energy states to this previously published level scheme. Spins were assigned up to $29/2^+$. The most recent and complete study (Sarantites) was in general agreement with the previous two, but differed from them in some important aspects. Three models were suggested to describe the nucleus: the weak-coupling model, the rotation aligned model (Stephens et al. 1973), and the cluster-core coupling model (Paar 1973). The latter was used extensively in the paper by Sarantites, and calculations based on it were compared with the experimental results.

However, there was no general concensus among the published works. The present work which was well underway when these papers appeared revealed additional discrepancies with them, and so further study was necessitated.

3.1 Gamma Ray Singles Measurements

The gamma ray spectrum resulting from the $(\alpha, 2n)$ reaction on ^{93}Nb using a beam energy of 27 MeV is presented in Figure 3.1. No lines pertinent to ^{95}Tc appear below 270 keV, and so this region is not shown. The impurities which appear as a result of competing reactions are identified in the figure. The energies and intensities of the transitions attributed to ^{95}Tc are tabulated in the first two columns of Table 3.1. The relative intensities at an excitation energy of 26 MeV were calculated using the A_0 coefficients, which were obtained by fitting an expansion of even order Legendre Polynomials to the angular distribution data for each gamma ray. These coefficients, the angular distribution effects having been removed, were then corrected for the efficiency of the detector. Relative singles intensities were also calculated using peak areas from a spectrum which was recorded at an angle of 55° to the beam axis. The results of these two methods agreed closely. The gamma rays were normalized to the strongest transition in the spectrum at 882.5 keV.

The third column in Table 3.1 gives the location of each transition in the level scheme.

Columns four and five present the experimental angular distribution coefficients, A_2 and A_4 . The sixth column gives the initial and final spins and parities assigned to the levels pertinent to the particular transition. Where it was not possible to assign a unique set of spins for a given transition, all acceptable results are presented.

FIGURE 3.1

The gamma ray spectrum of ^{95}Tc .

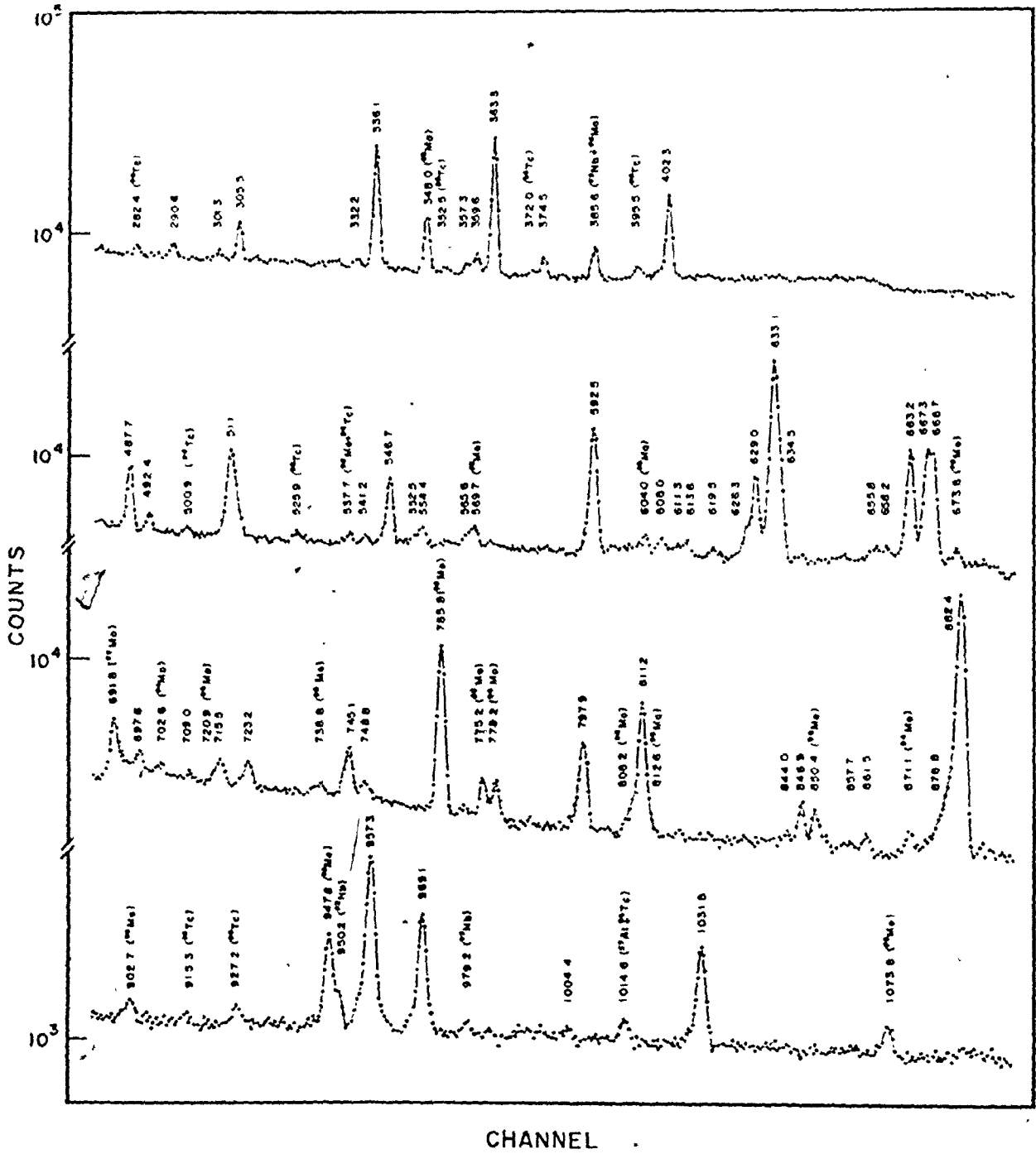


TABLE 3.1

Transitions on ^{95}Tc

Energy (keV)	Intensity	Classification	Expt'l Coefficients		Assignments $J_i^\pi - J_f^\pi$	Calculated Coefficients		
			A_2	A_4		A_2	A_4	$\tan^{-1}\delta$
290.6(1)	0.9(2)	627.0 \rightarrow 336.4	-.05(4)	-.00(4)	$5/2^+ \rightarrow 7/2^+$	-.05	.00	10
					$(7/2^+) \rightarrow 7/2^+$	-.05	-.00	-39
301.3(2)	0.7(1)	928.3 \rightarrow 627.0	.36(11)	.08(10)	$3/2^+ \rightarrow 5/2^+$.02	.00	-39
305.5(1)	3.1(2)	4127.6 \rightarrow 3822.1	.33(5)	.00(5)	$29/2^- \rightarrow 25/2^-$.40	-.05	3
					$27/2^- \rightarrow 25/2^-$.33	.03	20
336.4(1)	18.6(12)	336.4 \rightarrow 0.0	-.21(1)	.00(1)	$7/2^+ \rightarrow 9/2^+$	-.21	.00	59
359.6(3)	1.8(2)	2907.5 \rightarrow 2547.6	.48(14)	-.12(15)				
363.3(1)	24.4(14)	2547.6 \rightarrow 2184.3	-.23(1)	-.03(2)	$21/2^+ \rightarrow 19/2^+$	-.25	.00	-1
374.5(2)	1.9(2)	4293.5 \rightarrow 3919.0	-.45(9)	.26(11)	$31/2^+ \rightarrow 29/2^+$	-.24	.00	0
					$27/2^+ \rightarrow 29/2^+$	-.25	.00	2
397.5(10)	0.5(5)	1280 \rightarrow 882.5						
402.3(1)	11.4(8)	3919.0 \rightarrow 3516.7	.27(3)	-.16(3)	$29/2^+ \rightarrow 25/2^+$.26	-.15	-4

TABLE 3.1 (continued)

Energy (keV)	Intensity	Classification	Expt'l Coefficients		Assignments $J_i^\pi - J_f^\pi$	Calculated Coefficients		
			A_2	A_4		A_2	A_4	$\tan^{-1}\delta$
487.8(1)	9.2(6)	1702.0→1214.3	.19(3)	.05(4)	$13/2^- \rightarrow 9/2^-$.24	-.03	1
510.8(5)	5.3(13)	2213.0→1702.0			$17/2^- \rightarrow 13/2^-$			
546.8(1)	10.4(7)	1214.3→ 667.9	.10(3)	-.04(3)	$9/2^- \rightarrow 5/2^-$.09	-.03	-9
592.5(1)	21.5(25)	1549.8→ 957.3	.11(2)	-.04(2)	$15/2^+ \rightarrow 11/2^+$.15	-.09	-8
613.6(3)	1.8(3)	1281.5→ 667.9			$7/2^+ \rightarrow 5/2^-$			
626.3(5)	3.1(6)	627.0→ 0.0	.10(5)	-.06(5)	$5/2^+ \rightarrow 9/2^+$.03	.00	0
					$(7/2^+) \rightarrow 9/2^+$.08	.00	-22
629.0(1)	15.2(13)	667.9→ 38.9	.04(3)	-.00(3)	$5/2^- \rightarrow 1/2^-$.06	-.00	-6
633.1(1)	65.5(47)	1515.6→ 882.5	.24(1)	-.07(1)	$17/2^+ \rightarrow 13/2^+$.25	-.07	-2
634.5(1)	19.1(19)	2184.3→1549.8	.24(4)	-.14(4)	$19/2^+ \rightarrow 15/2^+$.20	-.12	-6
655.8(3)	1.5(3)	4783.3→4127.6						
663.2(1)	23.4(16)	2213.0→1549.8	-.10(2)	-.01(2)	$17/2^- \rightarrow 15/2^+$	-.10	.00	4_{-3}^{+2}
667.3(2)	20.0(15)	1549.8→ 882.5	.52(7)	.10(7)	$15/2^+ \rightarrow 13/2^+$.50	.07	51_{-28}^{+25}
668.7(2)	22.3(16)	2184.3→1515.6	.11(5)	-.09(6)	$19/2^+ \rightarrow 17/2^+$.04	.00	10

TABLE 3.1 (continued)

Energy (keV)	Intensity	Classification	Expt'l Coefficients		Assignments $J_i^\pi - J_f^\pi$	Calculated Coefficients		
			A_2	A_4		A_2	A_4	$\tan^{-1}\delta$
715.5(2)	2.9(2)	2231.1→1515.6	-.06(9)	-.09(10)				
723.2(1)	3.0(4)	2907.5→2184.3	.17(3)	-.04(4)				
745.1(2)	6.5(6)	1702.0→ 957.3	-.35(6)	.09(6)	$13/2^- \rightarrow 11/2^+$	-.28	-.00	-7^{+10} -10
748.8(4)	2.2(3)	1085.2→ 336.4			$7/2^+ \rightarrow 7/2^+$			
797.9(2)	10.4(9)	3822.1→ 3024.2	.23(4)	-.17(4)	$25/2^- \rightarrow 21/2^-$.22	-.16	-6^{+5} -4
811.2(1)	21.1(17)	3024.2→2213.0	.20(2)	-.09(3)	$21/2^- \rightarrow 17/2^-$.23	-.12	-5
844.0(3)	0.9(2)	1180.4→ 336.4	.04(9)	-.07(12)	$7/2^+ \rightarrow 7/2^+$			
877.8(2)	3.0(5)	1214.3→ 336.4	-.21(10)	-.13(11)	$9/2^- \rightarrow 7/2^+$	-.25	.00	-14^{+11} -76
882.5(1)	100.0(62)	882.5→ 0.0	.21(1)	-.06(1)	$13/2^+ \rightarrow 9/2^+$.20	-.04	-2^{+2} -2
957.3(1)	34.1(23)	957.3→ 0.0	-.40(2)	.10(2)	$11/2^+ \rightarrow 9/2^+$	-.37	.04	-64^0 -1
959.5(12)	1.6(3)	2475.1→1515.6	.07(11)	-.23(10)				
969.1(2)	16.2(13)	3516.7→2547.6	.26(4)	-.09(3)	$25/2^+ \rightarrow 21/2^+$.29	-.11	-2
973.6(6)	2.2(5)	1310.0→ 336.5	.45(20)	-.14(19)	$11/2^+ \rightarrow 7/2^+$			
1004.4(5)	0.9(3)	2706.4→1702.0	.30(23)	-.39(23)				
1031.8(2)	12.2(10)	2547.6→1515.6	.19(4)	-.02(4)	$21/2^+ \rightarrow 17/2^+$.24	-.01	-4

TABLE 3.1 (continued)

Energy (keV)	Intensity	Classification	Expt'l Coefficients		Assignments $J_i^\pi - J_f^\pi$	Calculated Coefficients		
			A_2	A_4		A_2	A_4	$\tan^{-1}\delta$
1214.6(3)	2.6(4)	1214.3→ 0.0	-.03(14)	.09(16)	$9/2^- \rightarrow 9/2^+$.02	-.01	-27
1237.5(5)	2.8(4)	2120.0→ 882.5						
1354.7(8)	1.0(10)	1691.1→ 336.4						

For each set of assigned spins, A_2 and A_4 coefficients can be deduced as a function of the mixing ratio δ and the population parameters of the initial state. It was assumed that all of the populations were gaussian possessing the same width σ . The appropriate value of σ was that which minimised the χ^2 for the angular distributions of a number of E2 transitions whose spins were known. This fit to these transitions was accomplished by setting $\delta=0$ and allowing σ to vary between 1.6 and 3.4. The best value for σ , established by these criteria was 3.0 ± 0.2 . Using the value 3.0 for the width of the gaussian, and assuming initial and final spins, the angular distribution data were then fitted as a function of the mixing ratio δ , which was varied from $\tan^{-1}_{-\infty}$ to \tan^{-1}_{∞} . The resulting A_2 and A_4 coefficients and the value of δ yielding a minimum χ^2 are shown in the last three columns. The only parameter allowed to float in the calculation was the A_0 term (intensity).

In most cases a unique initial spin could not be obtained solely from this calculation. However where a unique spin could be assigned with a 0.1% confidence limit, the upper and lower limits of the mixing ratio as well as the δ which gives the minimum χ^2 are shown. The χ^2 marking the 0.1% confidence limit for seven data points and one free parameter, that is six degrees of freedom is 3.743. The significance of this number is that there is only one chance in a thousand for a set of seven random points to yield a reduced χ^2 of 3.743 or less.

A correction for the solid angle of the detector was also included in the calculation. This correction was performed according to

the prescription of Camp and Van Lehn (1971), using a programme written by Krane (1972). The programme was intended for coaxial detectors but can be used for planar detectors by letting the inner radius approach zero. The crystal dimensions used in the calculation for the 14 cc planar Ge(Li) detector were: length 1.00 cm, outer radius 2.10 cm, inner radius 0.10 cm. The distance from the target to the crystal was 14.50 cm. Table 3.2 shows the solid angle correction coefficients, Q_2 and Q_4 as a function of gamma ray energy.

3.2 Gamma-Gamma Coincidence Results

The coincidence probabilities (c_{ij} 's) provide a method of establishing and checking a potential level scheme. In Table 3.3 are presented the c_{ij} 's for the direct cascades of the level scheme. The experimental c_{ij} 's are those observed using the number of coincidence events measured between two cascading transitions. The predicted c_{ij} 's are calculated using the proposed level scheme and the singles intensities measured for the transitions in the particular cascade. It should be noted here that the errors of the experimental c_{ij} 's are rather large. This is because the number of coincidences N_{ij} is statistical, the efficiencies of the two detectors have errors of approximately 5% each, and the N_0 term which is calculated from known cascades has an error of about 10%. Although in the close geometry of the gamma-gamma coincidence experiment the angular correlation effects are minimised, it is still possible to introduce discrepancies between the observed and predicted c_{ij} 's of 25% in unfavourable cases. However,

TABLE 3.2

Corrections for Detector Solid Angle

E_{γ} (keV)	Q_2	Q_4
100.	.9851	.9510
150.	.9853	.9516
200.	.9854	.9518
300.	.9854	.9520
500.	.9855	.9521
1000.	.9855	.9521
1500.	.9855	.9521

TABLE 3.3

Coincidence Probabilities

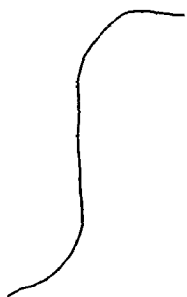
Cascade	c_{ij}	
	Expt'l	Predicted
633 + 634 - 882	78.2	71.7
1032 - 633	13.6	11.8
969 - 1032	4.9	5.1
402 - 969	6.8	9.7
375 - 402	1.6	1.6
667 + 669 - 882	69.3	42.3
669 - 633	14.2	22.1
363 - 669	16.3	13.7
969 - 363	10.6	10.8
360 - 363	1.4	1.6
360 - 1032	0.0	0.6
363 - 633 + 634	21.1	19.3
634 - 667	11.2	8.9
723 - 667 + 669	4.2	2.1
592 - 957	27.1	26.2
634 - 592	4.0	10.2
723 - 634	2.6	4.7
745 - 957	10.3	6.5
663 - 592	24.3	23.6

TABLE 3.3 (continued)

Cascade	c_{ij}	
	Expt'l	Predicted
488 - 1214	1.5	0.0
510 - 745	2.6	2.1
633 - 663	2.0	
811 - 663	21.6	19.4
546 - 629	9.6	9.3
488 - 546	5.5	6.4
510 - 488	2.3	3.2
811 - 510	2.9	2.5
798 - 811	7.5	11.4
305 - 798	2.7	2.7
655 - 305	0.8	1.4
488 - 878	2.5	3.0
1004 - 488	1.2	1.0
1004 - 745	0.0	0.6
878 - 336	7.1	4.4
614 - 629	2.7	1.8
290 - 336	1.2	0.9
301 - 290	0.0	0.2
301 - 626	1.2	0.5
749 - 336	1.4	2.2
844 - 336	0.0	0.9

TABLE 3.3 (continued)

Cascade	c_{ij}	
	Expt'l	Predicted
1355 - 336	1.1	1.0
398 - 882	1.0	0.5
1238 - 882	3.6	2.8
715 - 633	4.6	3.0
960 - 633	3.3	1.6



agreement to within about 20% for strong cascades can be expected; for weak transitions the error may be much larger. Comparing the two c_{ij} 's for a particular cascade, checks that the intensities of the gamma rays seen in coincidence are correct as proposed by the level scheme.

It was particularly difficult to calculate the c_{ij} 's for some of the cascades in the present work because there are at least two transitions at 633 keV and two more at 668 keV. Both doublets are separated by less than 1.5 keV, and all four transitions seemed to be closely related. Although an attempt was made to separate each component, interpretation of the gamma-gamma coincidence data was still extremely difficult.

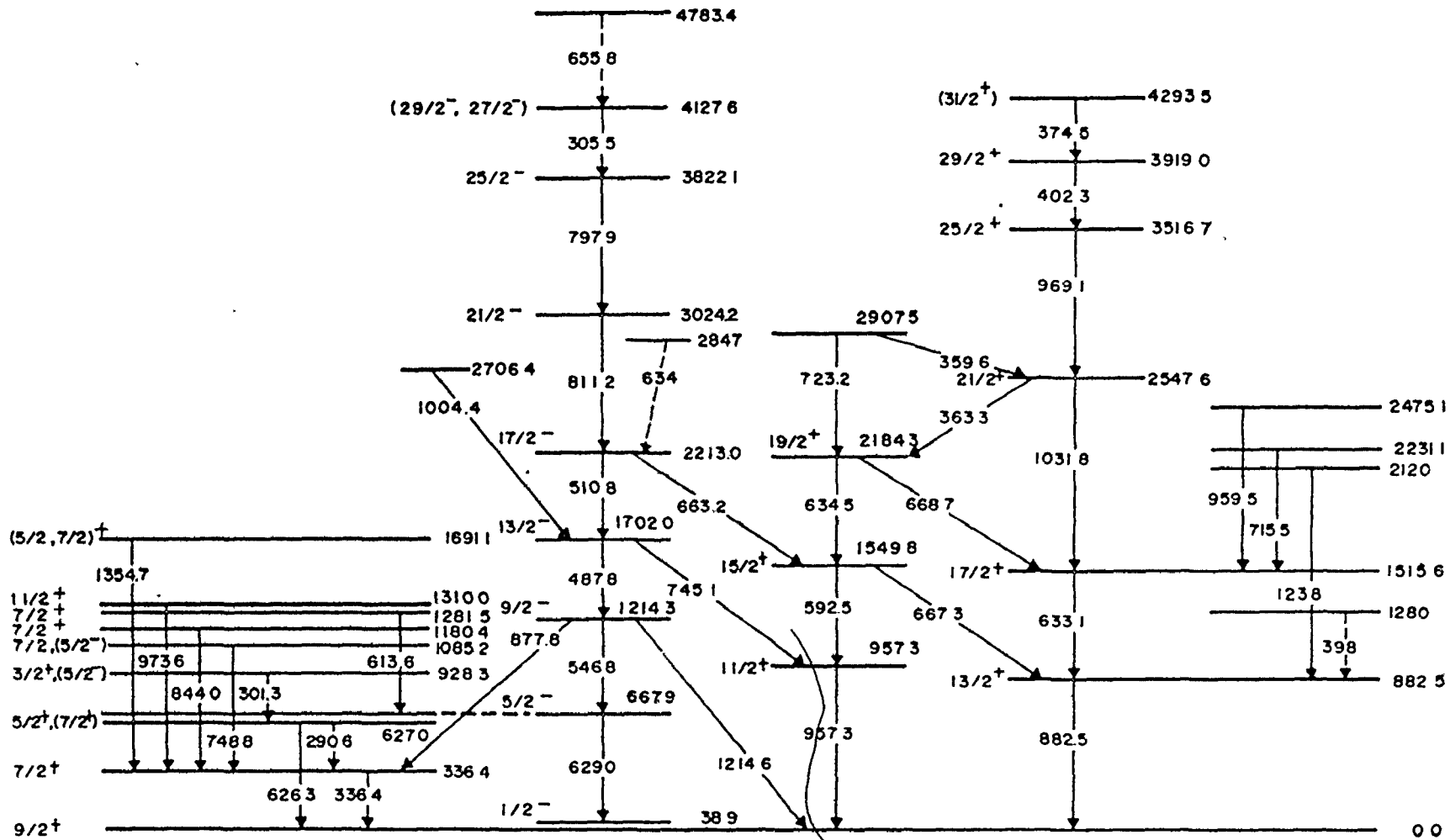
3.3 Presentation and Discussion of the Level Scheme

The results of the measurements described in the previous sections are incorporated into the level scheme of Figure 3.2. The level scheme has been drawn in such a way as to emphasise a striking feature: that is, its band structure. In constructing the scheme, coincidence evidence was always required before placing any transition.

The ground state and 38.9 keV isomeric state. These levels and their spins and parities have been well established (Madsen and Horen 1972, Xenoulis and Sarantites 1973, and Krämer and Huber 1973). The ground state results from a $(1g_{9/2})^3(2p_{1/2})^2$ configuration, and the isomeric state (half-life 61 days) from a $(1g_{9/2})^4(2p_{1/2})^1$ configuration. From the point of view of this investigation, the nucleus behaves as if

FIGURE 3.2

The level scheme of ^{95}Tc .



$^{95}\text{Tc}_{52}$

it has two ground states.

3.3.1 The Positive Parity Band

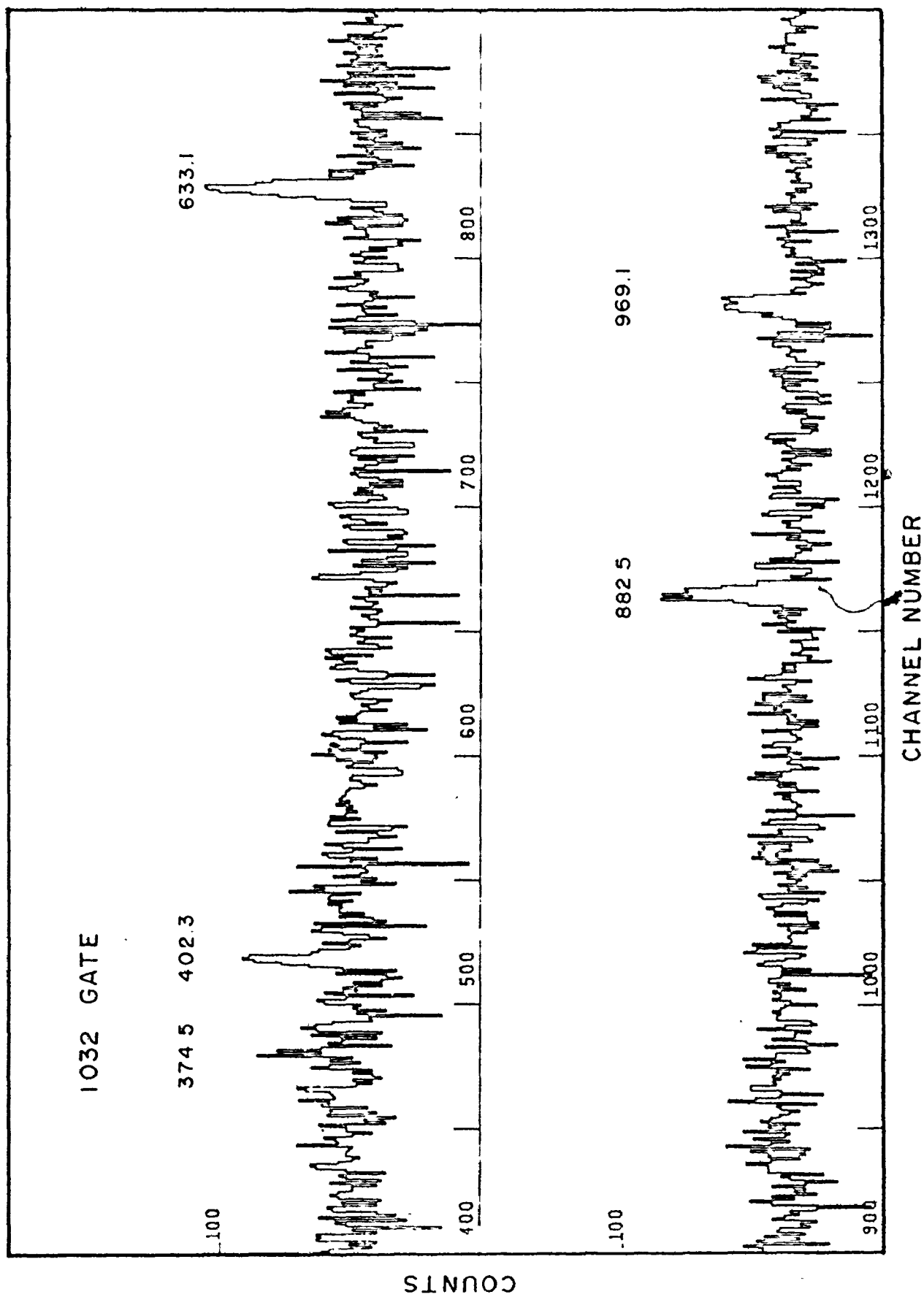
The 882.5, 1515.6, 2547.6, 3516.7, 3919.0, and 4293.5 keV levels.

This group of levels linked by six transitions shown in the 1032 keV coincidence gate of Figure 3.3, constitutes a positive parity band. The ordering of the transitions was determined from side-feeding transitions observed in the gamma-gamma coincidence work, from singles intensities, and from the excitation functions. The angular distributions of the transitions (882.5, 633.1, 1031.8, 969.1, 402.3, and 374.5 keV) and the results of the theoretical calculation are shown in Figure 3.4. For each transition the upper frame shows the best calculated fit to the experimental data, and the lower frame is a plot of the χ^2 as a function of the mixing ratio δ ($-90 < \tan^{-1} \delta < 90$). The values of δ for the five E2 transitions shown range from $\tan^{-2} 0$ to $\tan^{-4} 0$, and can be attributed to an inappropriate choice of σ . The five levels from 882.5 to 3919.0 keV have been assigned J^π values of $13/2^+$, $17/2^+$, $21/2^+$, $25/2$, and $29/2^+$. The 374.5 keV transition which de-excites the 4293.5 keV level is dipole in character, and its angular distribution restricts the spin of the level to $27/2$ or $31/2$. The data is not very good because a transition of this energy is also present in ^{96}Tc . The $31/2^+$ assignment is favoured, since a strong 776.8 keV transition to the 3516.7 keV level would be expected if the $27/2$ choice were made.

The excitation functions illustrate this band nicely, and are shown in Figure 3.5. The transitions have been corrected for the

FIGURE 3.3

The spectrum in coincidence with a gate set on the 1031.8 keV transition.



COUNTS

CHANNEL NUMBER

FIGURE 3.4

The angular distributions of the six transitions in the positive parity band.

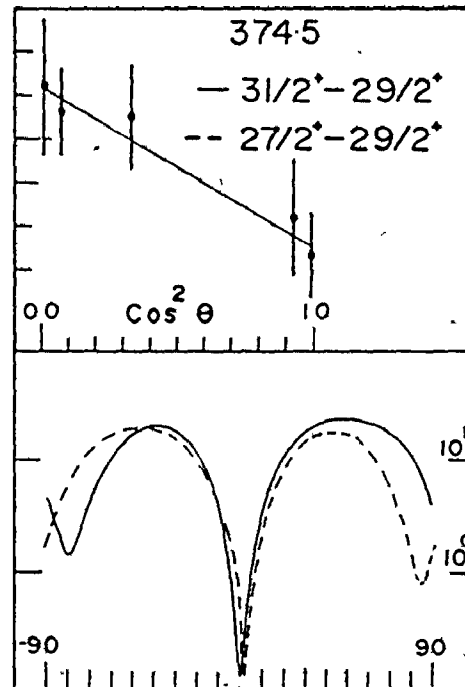
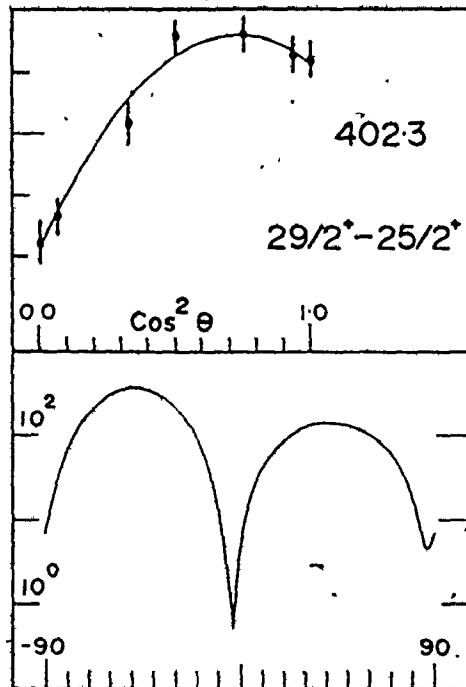
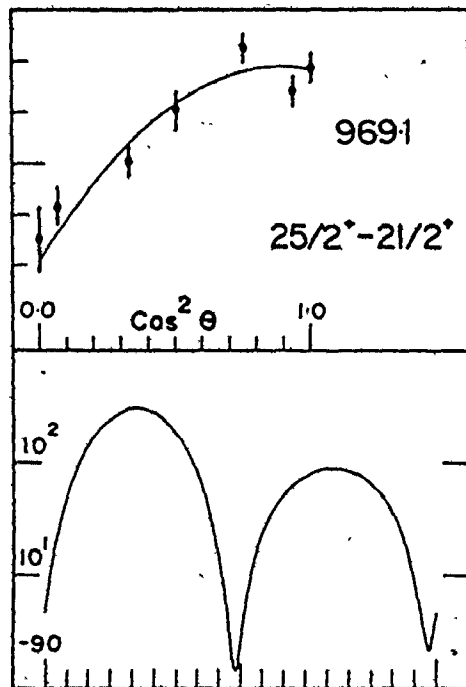
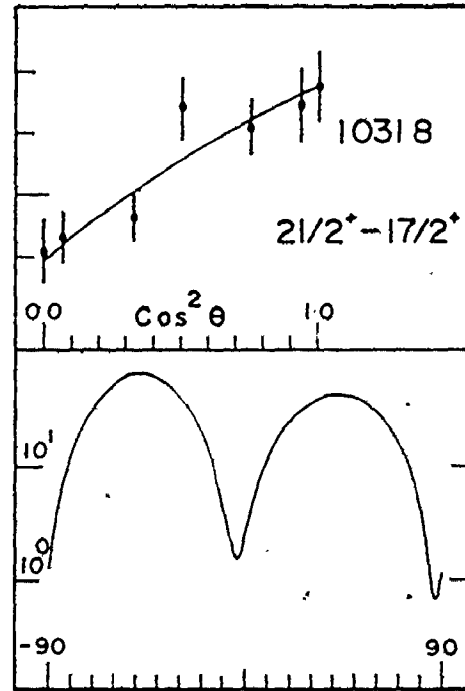
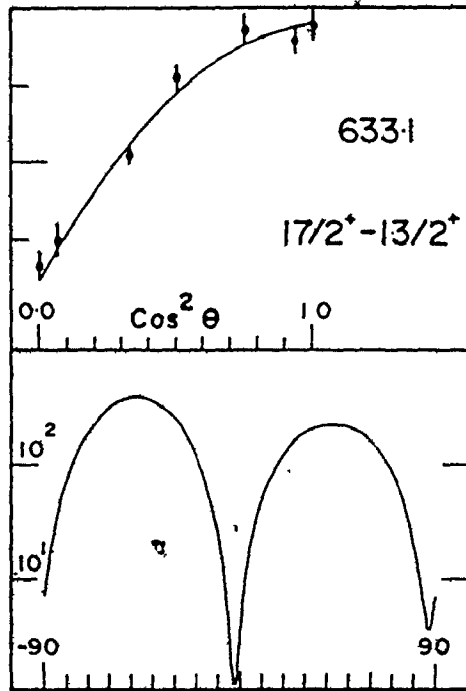
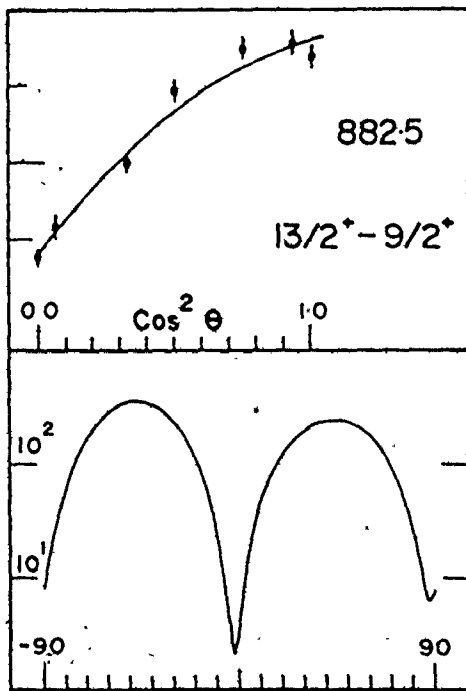
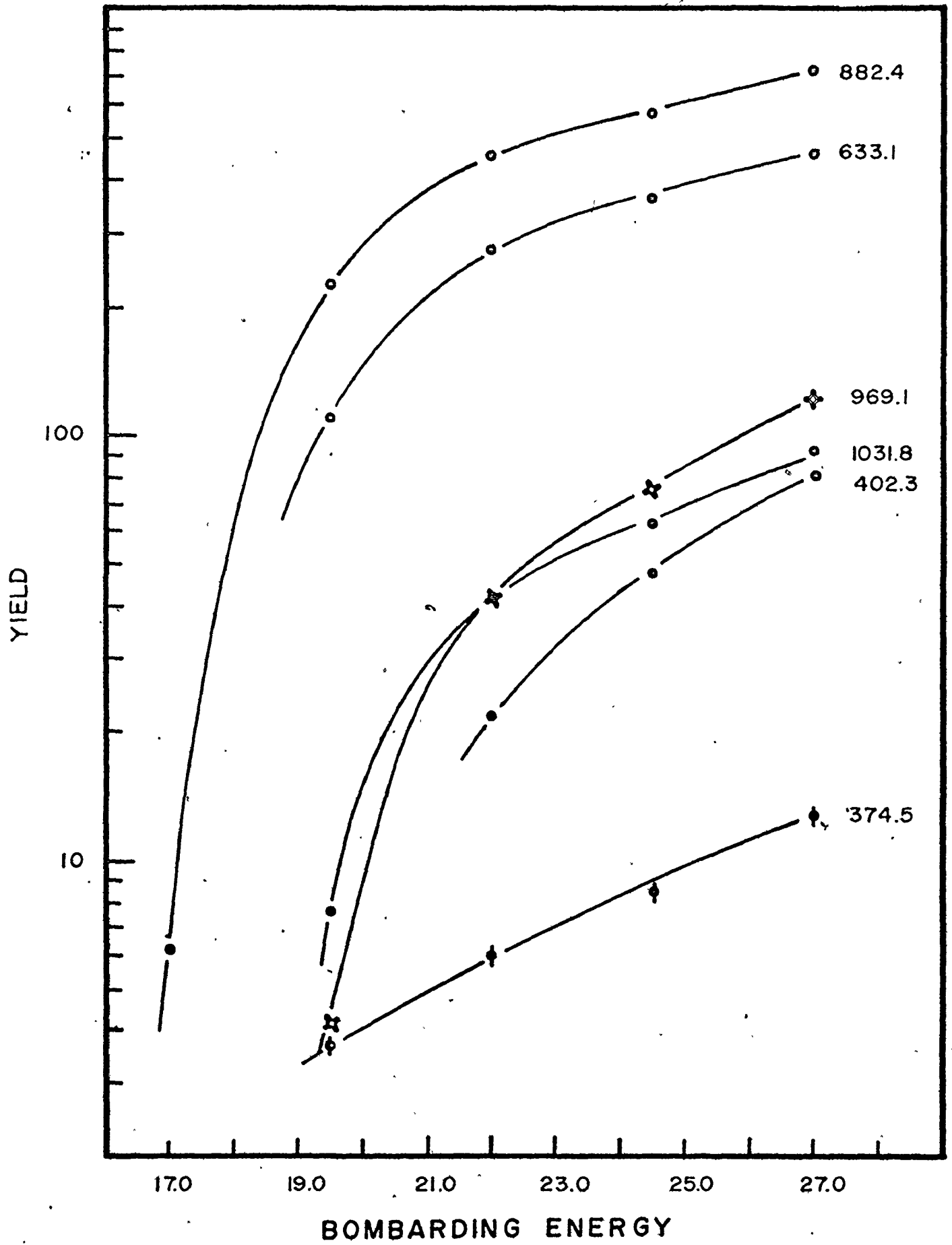


FIGURE 3.5

The excitation functions of the six transitions in the positive parity band.



efficiency of the detector, so that their yields are relative to the 882.5 keV transition. It can be seen that an increasing amount of energy is required to excite higher lying levels. The anomalous function for the 374.5 keV transition can be attributed to the presence of the ^{96}Tc component.

It should be noted here that the states with spins $25/2^+$, $29/2^+$, and $31/2^+$ cannot be formed by the $(\pi g_{9/2})^3$ configuration alone, but could be formed in configurations of the type $(\pi g_{9/2})^3(\nu g_{7/2})^2$ or $(\pi g_{9/2})^3(\nu d_{5/2})^2$.

The rotation aligned model is currently popular, and has been applied rather successfully to nuclei around mass 130 (Stephens *et al.* 1972). It may also prove to be useful in the discussion of lighter nuclei which exhibit collective natures. With this in mind, the rotation aligned picture was considered with respect to the bands in ^{95}Tc . The results were highly interesting.

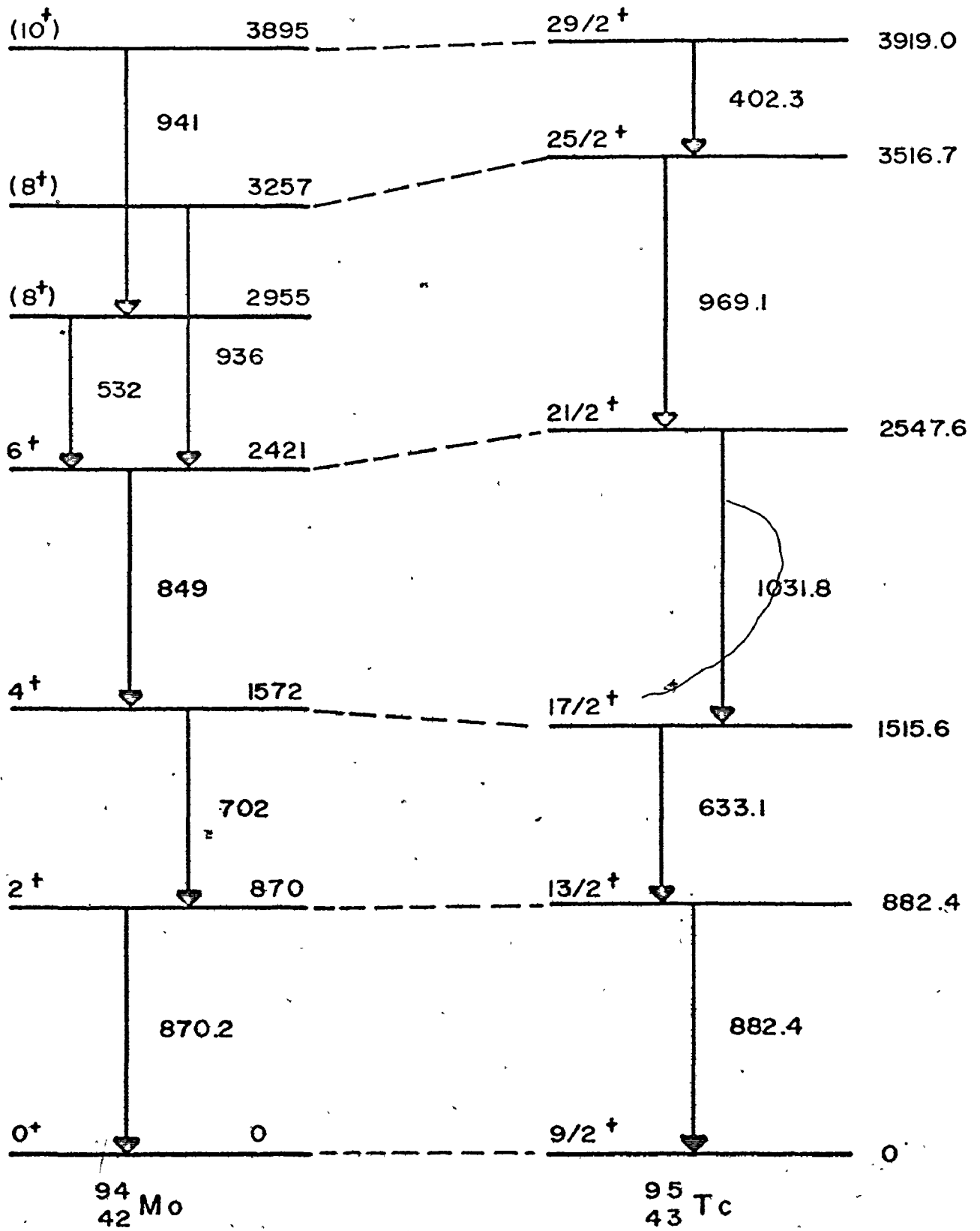
This positive parity band was compared with levels in ^{94}Mo , as shown in Figure 3.6. The comparison seems reasonable but difficulties exist concerning the relation of the $25/2^+$ level at 3516.7 keV to either of the 8^+ states in the ^{94}Mo core. However, the correspondence of the two nuclei was felt to be sufficiently good, to explain the positive parity band of ^{95}Tc in terms of the coupling of a $g_{9/2}$ proton to states in the ^{94}Mo core.

3.3.2 The Negative Parity Band

The 667.9, 1214.3, 1702.0, 2213.0, 3024.2, 3822.1, 4127.6, and 4783.4 levels. In a manner similar to the positive parity band, another

FIGURE 3.6

A comparison of the positive parity band of ^{95}Tc with levels in the core nucleus ^{94}Mo .



set of related levels was found. The members of this band are shown in two coincidence gated spectra. Figure 3.7 shows the transitions in coincidence with the 811.2 keV gamma ray. The 487.8 and 745.1 keV transitions de-excite the 1702.0 keV level and were therefore summed together to improve the statistics. This combined gated spectrum is shown in Figure 3.8.

In both coincidence gates a 510.8 keV line appears. This transition cannot be attributed to positron annihilation as the following argument shows. The results of the analysis of the spectrum in coincidence with the 511 keV gate are shown in Table 3.4. The first column lists all of the gamma rays appearing in this spectrum. The second column tabulates the measured coincidence intensities of these transitions, corrected for detector efficiency. The third column presents the relative singles intensities, normalized in such a way that all of the observed intensity of the very strong 882.5 keV line is due to chance. It can be seen that for the gamma rays which appear in Figures 3.7 and 3.8, the experimental intensities of Table 3.4 are much too strong to be due to chance alone. Unfortunately, neither excitation functions nor angular distributions could be obtained for the 510.8 keV transition, since it was masked by the 511.0 keV annihilation peak in all singles experiments. The singles intensity in Table 3.1 was estimated from the coincidence results. None of the published works have identified the existence of the 510.8 keV transition, which plays an important role in the decay scheme.

FIGURE 3.7

The spectrum in coincidence with a gate set on the 811.2 keV photopeak.

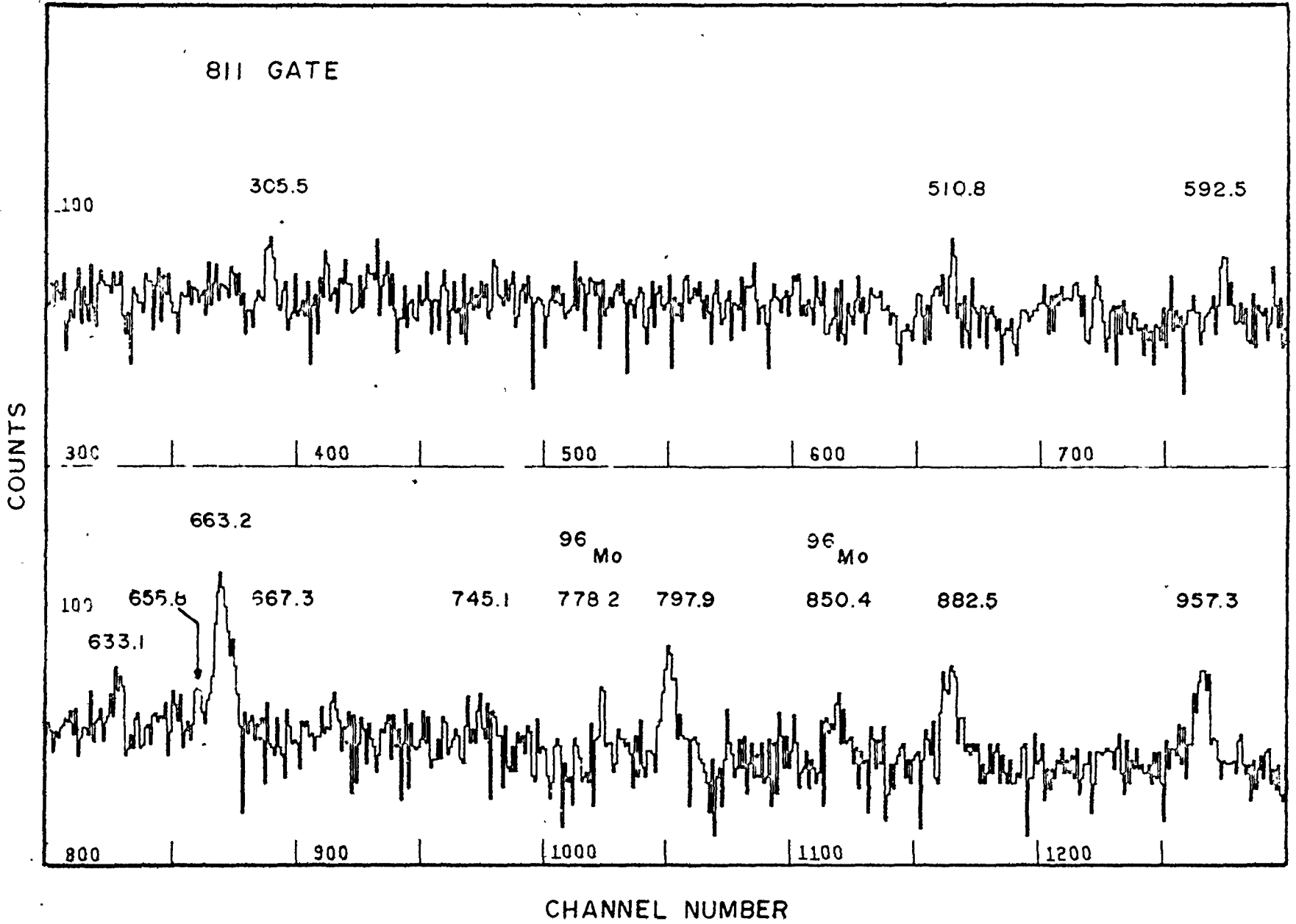


FIGURE 3.8

The spectrum in coincidence with the sum of gates set on the
487.8 and 745.1 keV photopeaks.

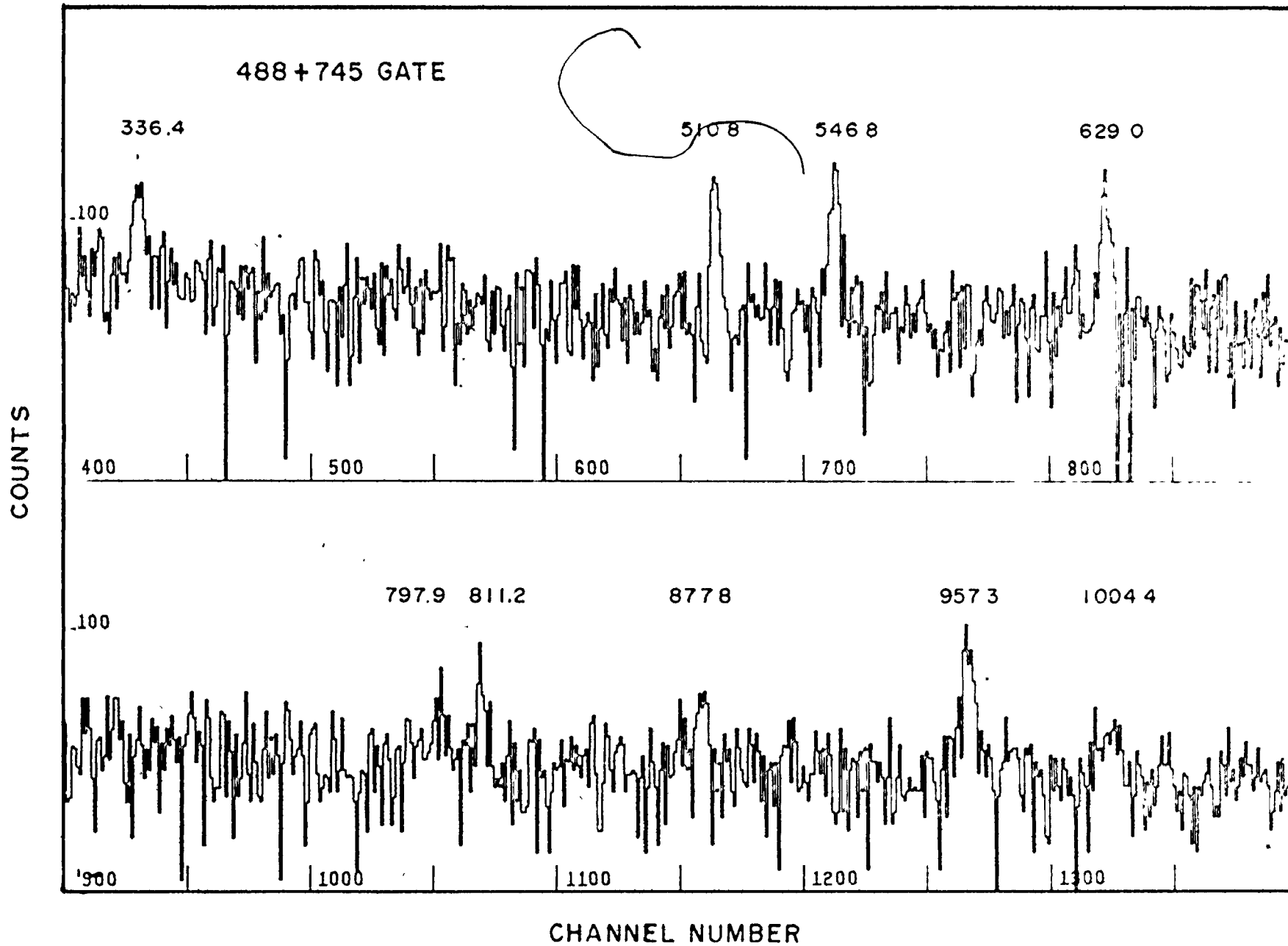


TABLE 3.4

Gamma Rays Appearing in Coincidence with the 510.8 keVGamma Ray Transition

E_{γ} (keV)	Expt'l Intensity	γ -Annihilation Chance Intensity	Evidence for γ -510.8 Coincidences
336.4	24(3)	7.4(5)	Yes
487.8	30(4)	3.7(2)	Yes
546.8	20(8)	4.2(3)	Yes
629.0	31(7)	6.1(5)	Yes
633.1 + 634.5	42(10)	33.8(24)	No
667.3 + 668.7	20(6)	16.9(12)	No
745.1	34(6)	2.6(2)	Yes
811.2	31(6)	8.4(7)	Yes
877.8	18(5)	1.2(2)	Yes
882.5	40(6)	40.0(25)	No
957.3	37(6)	13.6(9)	Yes

Figure 3.9 shows the angular distributions of the 629.0, 546.8, 487.8, 811.2, 797.9, and 305.5 keV transitions. Because the target nucleus has spin $9/2^+$, the angular distributions of the low spin transitions (629.0 and 546.8 keV) are somewhat attenuated.

The 667.9 level has been observed from the (p,n) reaction to de-excite by an E2 transition to the 38.9 keV isomeric state, thereby establishing a J^π value of $5/2^-$ (Kim et al. 1971, Sarantites and Xenoulis 1974).

The $9/2^-$ assignment to the 1214.3 keV level is based on the angular distributions of the 546.8 keV transition (Figure 3.9) and the 877.8 and 1214.6 keV transitions (Figure 3.10).

Similarly the $13/2^-$ assignment to the 1702.0 keV level depends on the angular distributions of the 487.8 and 745.1 keV transitions (Figures 3.9 and 3.10).

The 510.8 keV transition previously discussed, forms the link between these levels and the higher members of the band. This transition defines a level at 2213.0 keV. The angular distribution of the 663.2 keV transition (Figure 3.10) limits the value of J^π to $17/2^\pm$ or $13/2^\pm$, and the presence of the 510.8 keV transition further restricts the choice to $17/2^-$ or $13/2^\pm$. With a $13/2$ choice, a number of energetically favoured transitions would be expected, which are conspicuous here only by their absence. Since the ($\alpha, 2n$) mechanism deposits a large amount of angular momentum in the compound nucleus, the spins of the levels are expected to decrease as the excitation chain is descended.

FIGURE 3.9

The angular distributions of six transitions in the negative parity band.

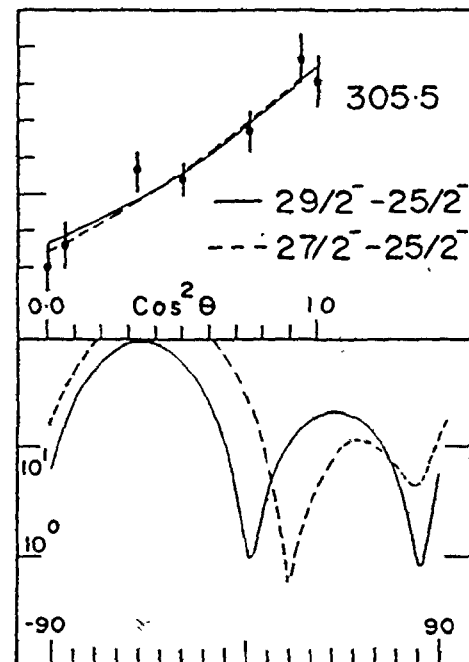
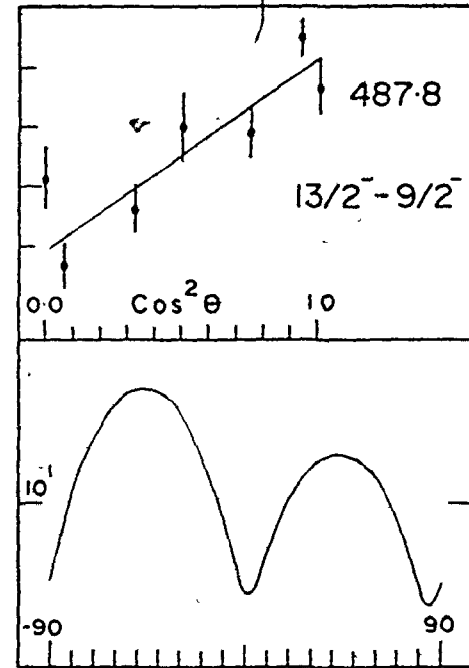
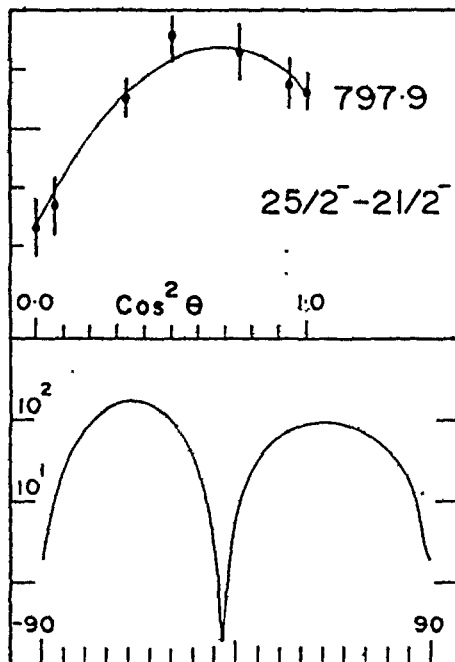
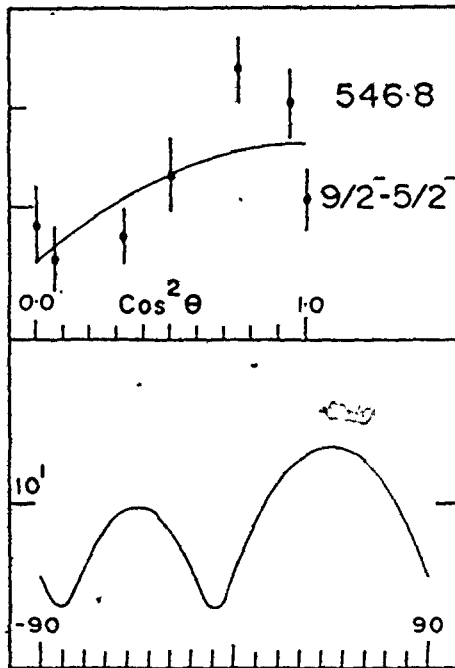
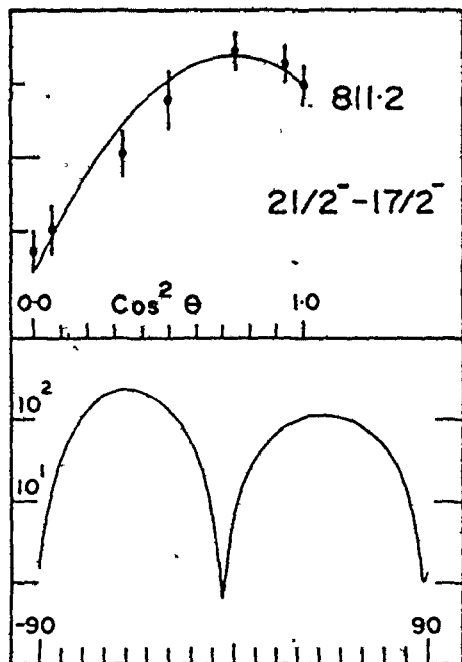
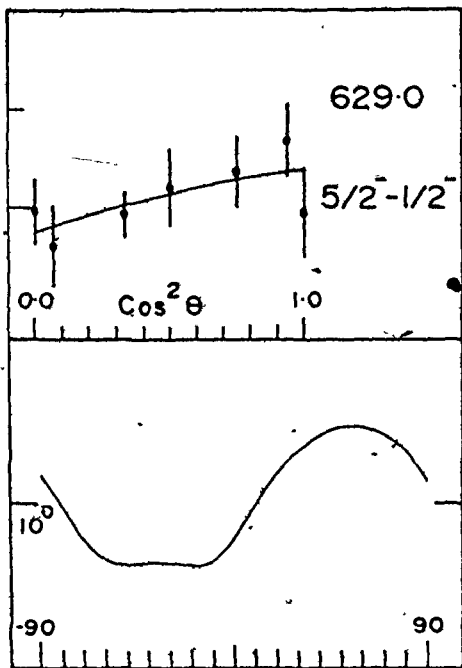
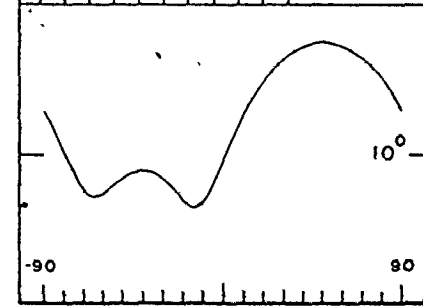
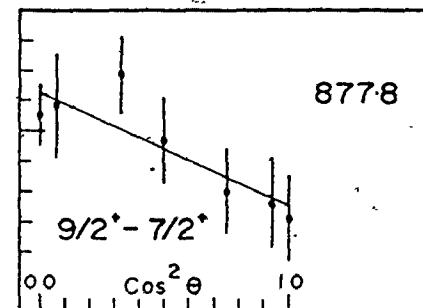
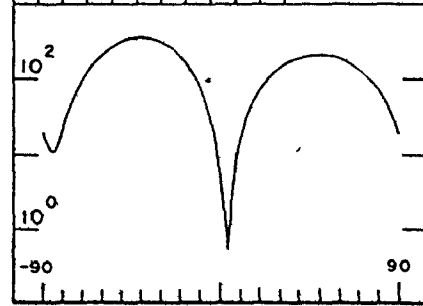
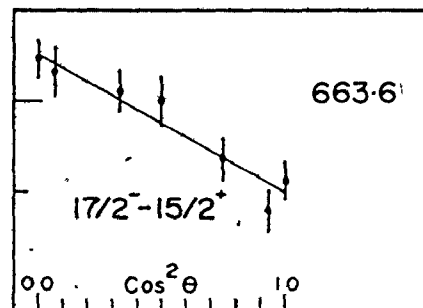
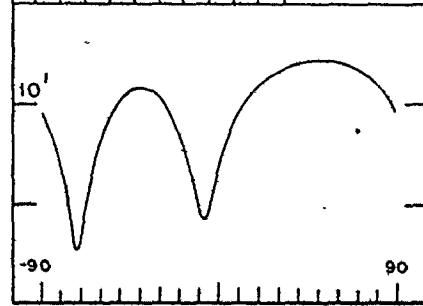
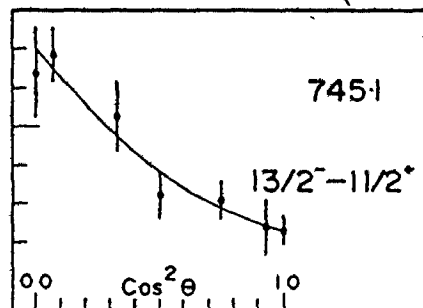
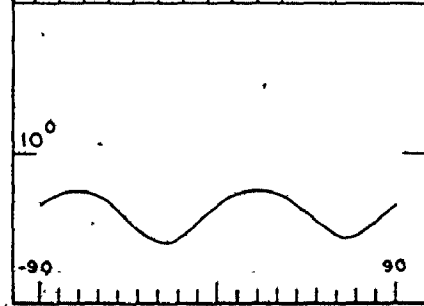
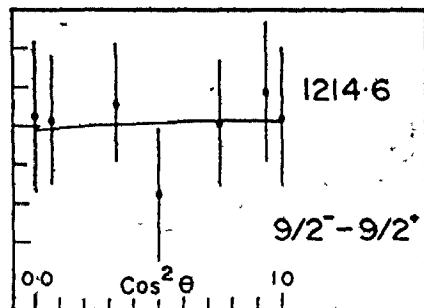
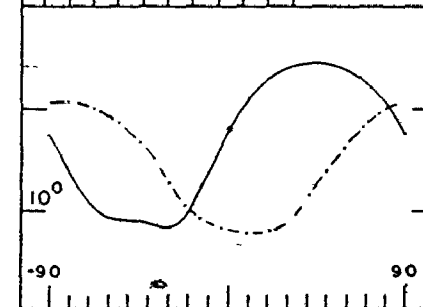
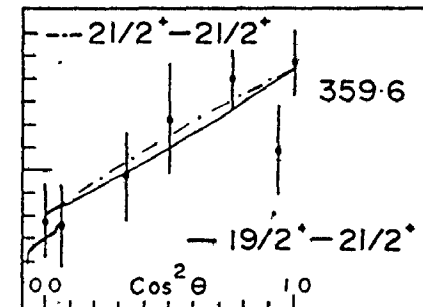
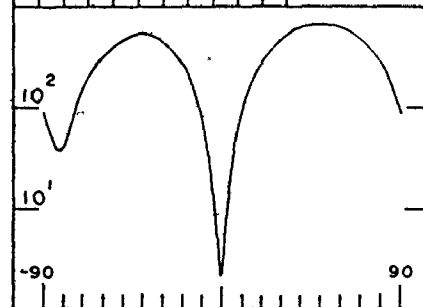
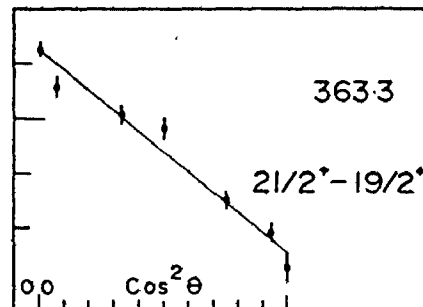
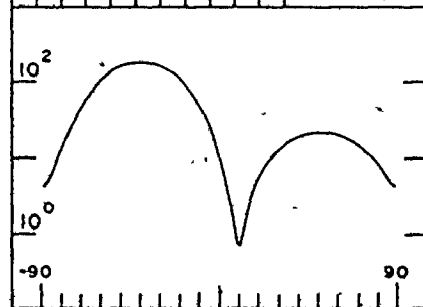
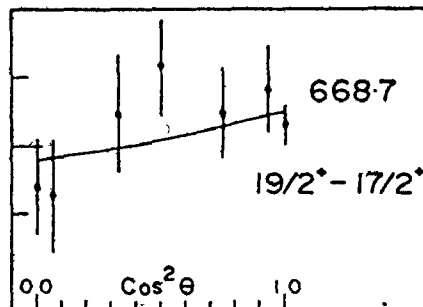
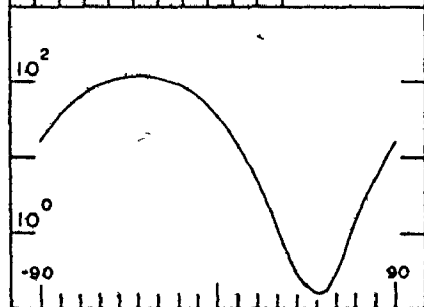
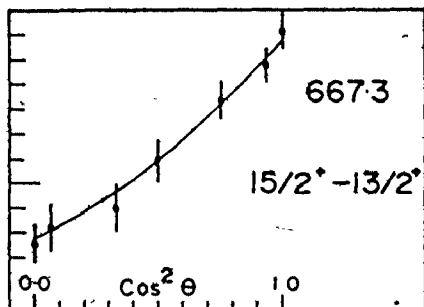


FIGURE 3.10

The angular distributions of eight transitions which effect connections with the two major bands.



The 811.2 and 797.9 keV transitions establish levels at 3024.2 and 3822.1 keV. These transitions are E2; the levels were assigned J^π values of $21/2^-$ and $25/2^-$ respectively.

From the coincidence data the 305.5 and 655.8 keV transitions were placed, establishing levels at 4127.6 and 4783.4 keV. The angular distribution of the 305.5 keV transition suggests a J^π value of either $29/2^-$ or $27/2^-$. No angular distribution was obtained for the 655.8 keV transition. However if they are both parts of the band, the 4127.6 and 4783.4 keV levels would be expected to have J^π values of $29/2^-$ and $33/2^-$ respectively.

The excitation functions for the negative parity band are shown in Figure 3.11. Again it can be seen that increasing amounts of excitation energy are required to populate higher lying levels. The excitation function of the 655.8 keV transition has not been shown, since an impurity of that energy from ^{93}Nb masks the ^{95}Tc line.

The correspondence between the levels of this band and levels in ^{96}Mo is shown in Figure 3.12. It appears that the rotation aligned model may be applied here as well. When the level energies are plotted as a function of $J(J+1)$, as seen in Figure 3.13 smooth curves result, indicative of band structure. It is apparent that the yrast levels in ^{96}Mo come from two different bands: one of which is based on the 0^+ ground state, the other on the first excited 0^+ level. When the negative parity band of ^{95}Tc is compared with the latter band, there is a striking similarity. This result further confirms the existence of the negative parity band, its spins and parities. It may be explained in

FIGURE 3.11

The excitation functions of six transitions in the negative parity band.

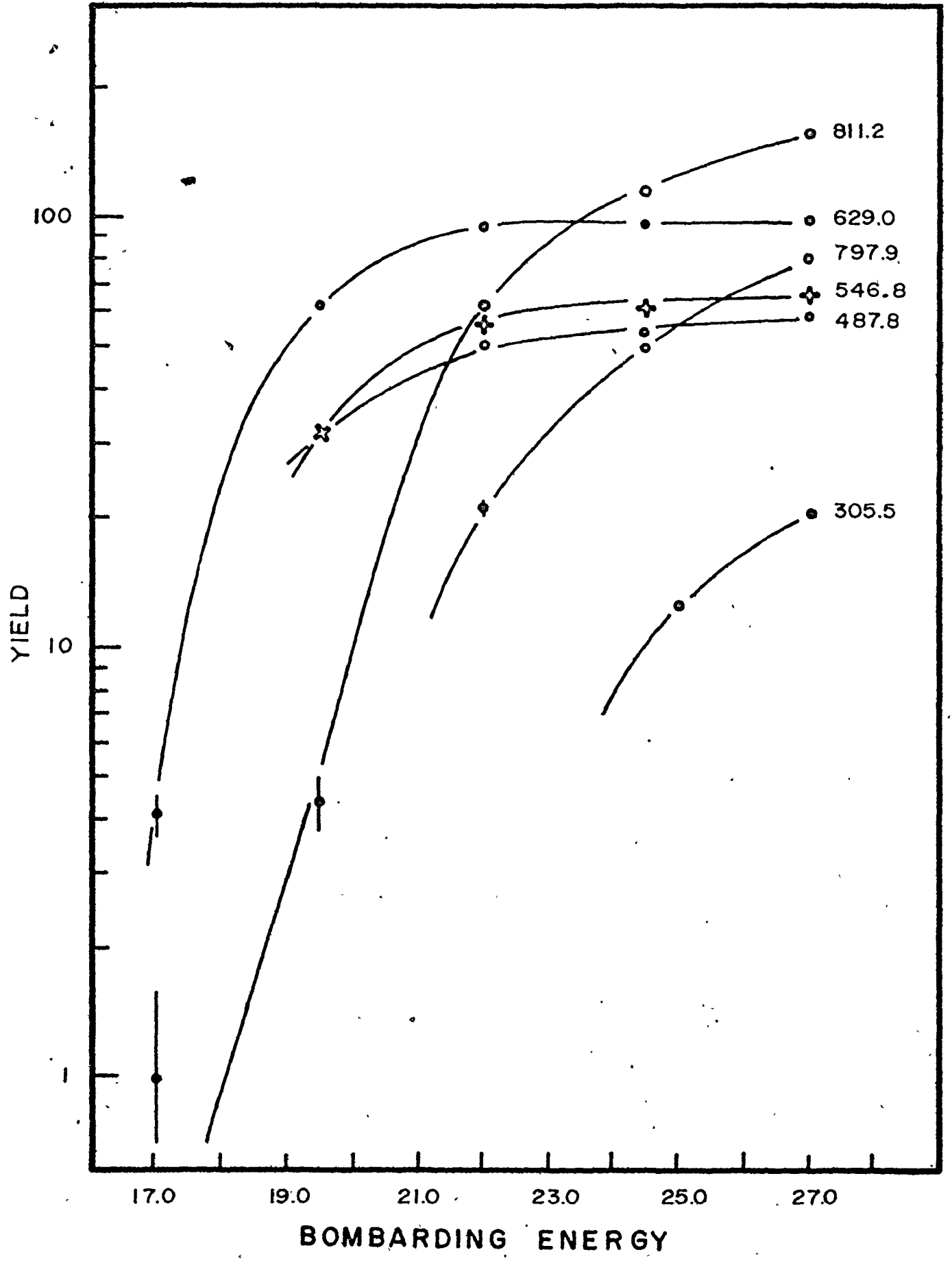


FIGURE 3.12

A comparison of the negative parity band of ^{95}Tc with levels
in the nucleus ^{96}Mo .

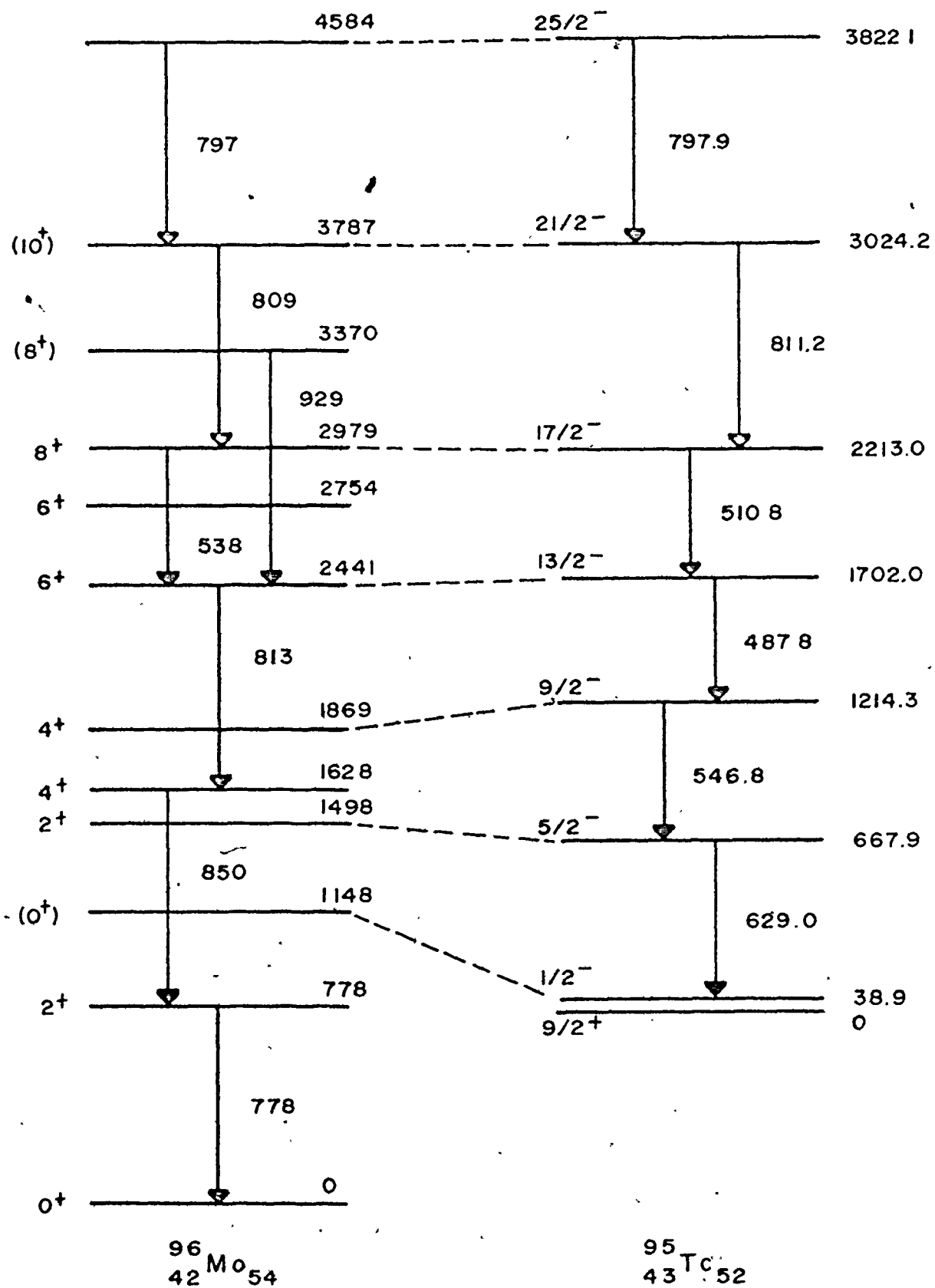
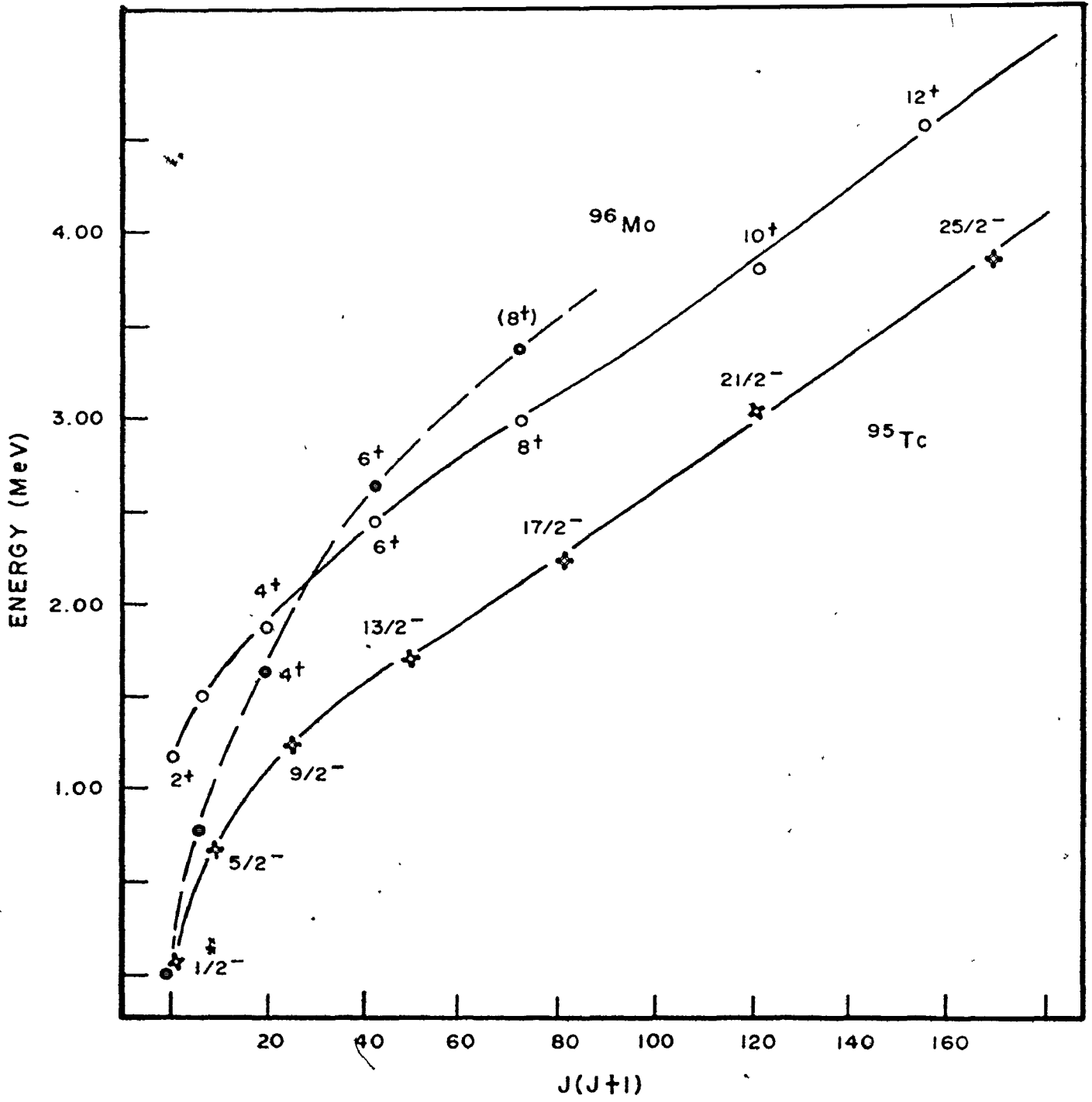


FIGURE 3.13

A plot of energy as a function of $J(J + 1)$ showing the negative parity band of ^{95}Tc and two bands of ^{96}Mo .



terms of the coupling of a $p_{1/2}$ proton to something which resembles an excited ^{96}Mo core. It would have been preferable to make the comparison with the ^{94}Mo core. Unfortunately neither the 0^+ excited state nor the band based on it have been identified.

Two additional levels are presented here, whose transitions feed levels in the negative parity band. The 2706.4 keV level is proposed on the basis of 487.8 - 1004.4 keV coincidences. The 1004.4 keV transition was too weak to give a useful angular distribution. The 2847 keV level is proposed on the basis of 663.2 - 634 keV coincidences. This introduces a third transition at approximately 633 keV, but its intensity need only be 2.4% to give the correct intensity balance. Sarantites (1975) placed the 663.2 keV transition on top of the 2184.3 keV level, thus creating a level at 2847 keV. However his assignment fails to give the correct intensity balance, and does not account for the observed coincidences with the 811.2 and 797.9 keV transitions.

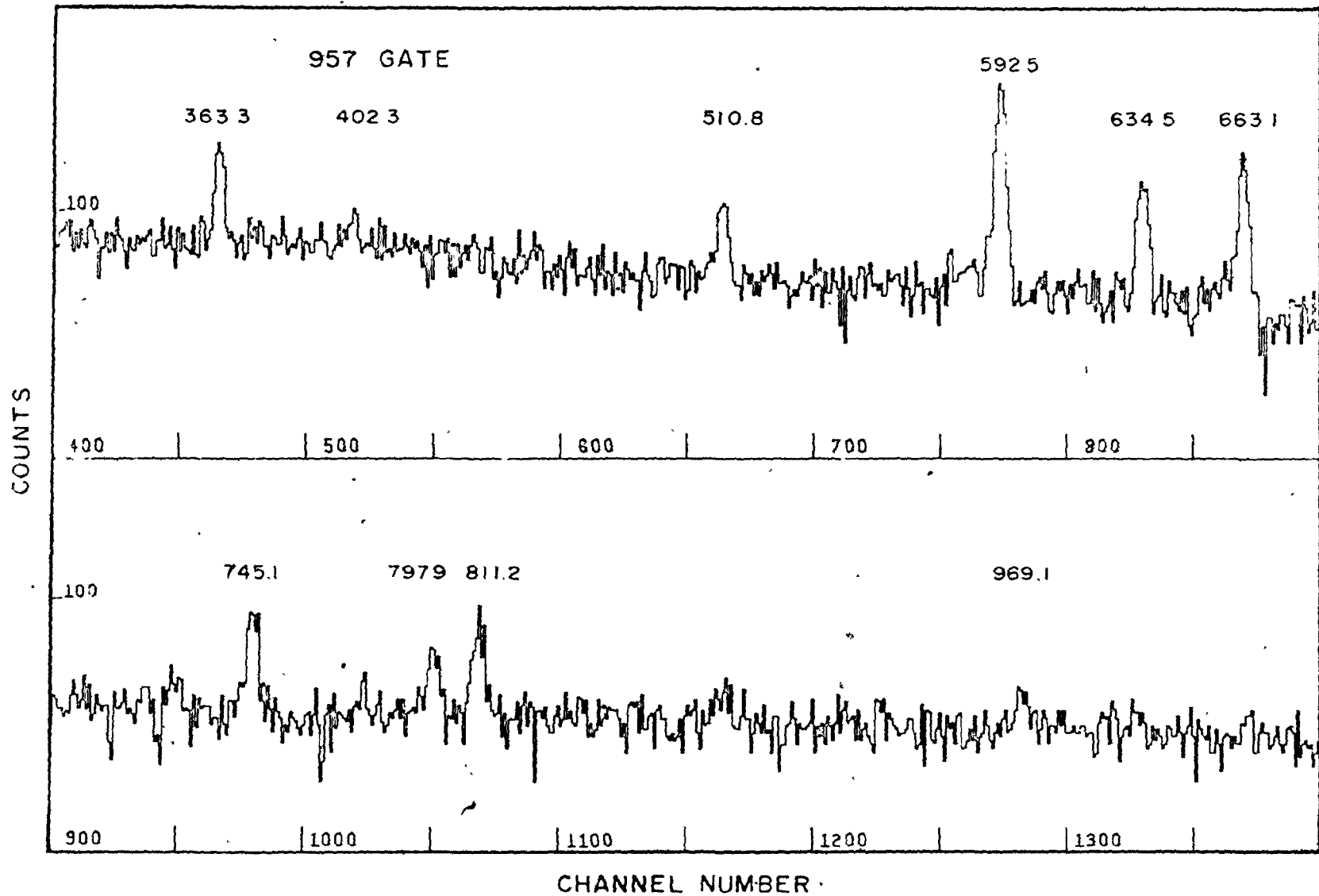
3.3.3 The 957.3, 1549.8, 2184.3, and 2907.5 keV Levels

These levels are connected by transitions to the major positive and negative parity bands, as shown by the spectrum in coincidence with the 957.3 keV transition (Figure 3.14). It is not clear from the present work whether they form a separate band or are merely part of the major positive parity levels. Their properties are discussed in turn.

The 1549.8 keV level decays by an E2 transition to the $11/2^+$ 957.3 keV level, and by an M1/E2 transition (Figure 3.10) to the $13/2^+$

FIGURE 3.14

The spectrum in coincidence with a gate set on the 957.3 keV photopeak.



882.5 keV level. Its J^π value is therefore concluded to be $15/2^+$.

Similarly the 2184.3 keV level decays to the $15/2^+$ 1549.8 keV level by an E2 transition, and to the $17/2^+$ 1515.6 keV level by an M1/E2 transition (Figure 3.10). Thus a $19/2^+$ assignment has been given to the level. The presence of a pure M1 transition of energy 363.3 keV (Figure 3.10) which depopulates the $21/2^+$ 2547.6 keV level of the positive parity band further supports the assignment.

The 2907.5 keV level is de-excited by the weak 359.6 and 723.2 keV transitions, and no unique spin assignment is possible from the angular distribution data. The favoured solutions for the 359.6 keV transition are shown in Figure 3.10.

3.3.4 The Shell Model Levels

The 336.4, 627.0, 928.3, 1085.2, 1180.4, 1281.5, 1310.0, and 1691.1 keV levels. These levels have been well established from the decay of ^{95}Ru , and from the (p,n) reaction on ^{95}Mo (Xenoulis and Sarantites 1973, Krämer and Huber 1974, and Sarantites and Xenoulis 1974). The present work concurs with these results. However the levels are populated very weakly since they possess low spins, and the $(\alpha, 2n)$ reaction preferentially populates high spin levels. The J^π values shown in Figure 3.2 and in Table 3.1 are those adopted by previous workers, since no conclusive results were obtained for them from the present angular distribution measurement. The A_2 and A_4 coefficients, and values for δ shown in Table 3.1 are those for which the χ^2 of the model fit was minimum.

These levels have been discussed within the framework of the shell model (Vervier 1966, Bhatt and Ball 1965), and will not be dealt with further in this work.

3.3.5 The 1280, 2120, 2231.1, and 2475.1 keV levels

These levels are proposed on the basis of the gamma-gamma coincidence measurements. Coincidence events between the 882.5 and 398 keV transitions suggest a level at 1280 keV; those between the 882.5 and 1238 keV transitions are a basis for the 2120 keV level. The 2231.1 and 2475.1 keV levels are proposed as a result of 882.5, 633.1, and 715.5 keV coincidences, and 882.5, 633.1, and 959.5 keV coincidence events respectively. Spin and parity assignments for the levels could not be established.

3.4 Comparison with Other Workers

The present measurements regarding the positive parity band confirm the conclusions of other workers. Shibata et al. (1974) reported the levels at 882.5, 1515.6, and 2547.6 keV. Hippe et al. (1975) added the levels 3516.7 and 3919.0 keV, and Sarantites (1975) observed the complete band.

The negative parity band has not been reported as such. The 667.9, 1214.3, and 1702.0 keV levels were observed in the previous papers, however the connection between these levels and the higher band members by way of the 510.8 keV transition was not established. The spins and parities of the upper band levels have been determined from the present work.

The 957.3, 1549.8, 2120, 2184.3, 2231.1, 2475.1, and 2907.5 keV levels reported in this work confirm the results of the other workers using the $(\alpha, 2n)$ reaction.

3.5 Subsequent Investigations

Although there have been many experiments investigating the nucleus ^{95}Tc , it is apparent that the last word has not been said.

Internal conversion experiments are currently under investigation, which may reveal the multipolarities of those dipole transitions which are undetermined. Preliminary results have shown that despite the low atomic number (43) and the small internal conversion coefficients, the yields are sufficiently large to obtain meaningful data. The average ratio of the peak height to background is 2.5 to 1. The internal conversion measurements have further verified the existence of the 510.8 keV transition in ^{95}Tc .

The nucleus may also be populated using lithium induced reactions. The Q-value of the $^{92}\text{Zr}(^6\text{Li}, 3n)^{95}\text{Tc}$ reaction is -12.6 MeV, and of the $^{92}\text{Zr}(^7\text{Li}, 4n)^{95}\text{Tc}$ reaction is -19.8 MeV. The latter reaction may be more fruitful since more energy is carried into the system. Because more angular momentum and excitation energy is introduced by the lithium ions, levels of high spin and excitation will be preferentially populated. Therefore, the band structure of the nucleus will be accentuated. These experiments are in preparation.

Other reactions using heavier projectiles are not practical because too much excitation energy is required to surmount the coulomb

barrier.

In summary, the rotation aligned model has been found to explain with reasonable success, the high spin states of ^{95}Tc studied in this work.

REFERENCES

- Auerbach, N., and Talmi, I. (1965). Nucl. Phys. 64, 458.
- Bhatt, K. H., and Ball, J. B. (1965). Nucl. Phys. 63, 286.
- Camp, D. C., and Van Lehn, A. L. (1969). Nucl. Instr. Meth. 76, 192.
- Cook, W. B., Schellenberg, L., and Johns, M. W. (1969). Nucl. Phys. A139, 277.
- Cook, W. B., Johns, M. W., Geiger, J. S., and Graham, R. L. (1972). Can. J. Phys. 50, 1511.
- Cook, W. B., and Johns, M. W. (1972). Can. J. Phys. 50, 1957.
- Cook, W. B. (1972). Ph.D. Thesis, McMaster University.
- Graham, R. L., Geiger, J. S., and Johns, M. W. (1972). Can. J. Phys. 50, 513.
- Hippe, D., Heits, B., Schuh, H.-W., Zell, K. O., Friederichs, H.-G., and von Brentano, P. (1975). Z. Physik. A273, 349.
- Kim, H. J., Robinson, R. L., Johnson, C. H., and Raman, S. (1970). Nucl. Phys. A142, 35.
- Kim, H. J., Robinson, R. L., and Johnson, C. H. (1971). Nucl. Phys. A167, 65.
- Krämer, K., and Huber, W. (1973). Z. Physik. 267, 117.
- Krane, K. S. (1972). Nucl. Instr. Meth. 98, 205.
- Lederer, C. M., Hollander, J. M., and Perlman, I. (1967). "Table of Isotopes," sixth ed., John Wiley and Sons, New York, New York.

- Lederer, C. M., Jaklevic, J. M., and Hollander, J. M. (1971). Nucl. Phys. A169, 449.
- Lederer, C. M., Jaklevic, J. M., and Hollander, J. M. (1971). Nucl. Phys. A169, 489.
- Medsker, L. R., and Horen, D. J. (1972). Nucl. Data B8, 29.
- Nuclear Data Sheets (1971). B5, 321.
- Nuclear Data Sheets (1972). B8, 29.
- Nuclear Data Sheets (1972). B8, 527.
- Nuclear Data Sheets (1973). 10, 241.
- Paar, V. (1973). Nucl. Phys. A211, 29.
- Preston, M. A. (1962). "Physics of the Nucleus," Addison-Wesley Co. Inc., Reading, Mass.
- Sarantites, D. G., and Xenoulis, A. C. (1974). Phys. Rev. C10, 2348.
- Sarantites, D. G. (1975). Phys. Rev. C12, 1176.
- Shibata, T., Itahashi, T., and Wakatsuki, T. (1974). Nucl. Phys. A237, 382.
- Stephens, F. S., Diamond, R. M., Leigh, J. P., Kamuri, T., and Nakai, K. (1972). Phys. Rev. Lett. 29, 438.
- Stephens, F. S., Diamond, R. M., and Nilsson, S. G. (1973). Phys. Lett. 44B, 429.
- Stephens, F. S. (1975). Rev. Mod. Phys. 47, 43.
- Tucker, A. B., and Hein, W. W. (1970). Nucl. Phys. A155, 129.
- Vervier, J. (1966). Nucl. Phys. 75, 17.
- Xenoulis, A. C., and Sarantites, D. G. (1973). Phys. Rev. C7, 1193.
- Yamazaki, T. (1967). Nuclear Data A3, 1.